Journal of Cosmology and Astroparticle Physics
An IOP and SISSA journal

Received: June 14, 2024
Accepted: September 24, 2024
Published: October 25, 2024

Formation and decay of oscillons after inflation in the presence of an external coupling. Part I. Lattice simulations

Mohammed Shafi,[a] **Edmund J. Copeland**,[b] **Rafid Mahbub**,[c] **Swagat S. Mishra**[b] **and Soumen Basak**[a]

[a]*School of Physics, Indian Institute of Science Education and Research, Thiruvananthapuram, 695551, India*
[b]*School of Physics and Astronomy, University of Nottingham, Nottingham, NG7 2RD, U.K.*
[c]*Department of Physics, Gustavus Adolphus College, Saint Peter, MN 56082, U.S.A.*
E-mail: mohammedshafi18@alumni.iisertvm.ac.in, edmund.copeland@nottingham.ac.uk, mahbub@gustavus.edu, swagat.mishra@nottingham.ac.uk, sbasak@iisertvm.ac.in

Abstract: We investigate the formation and decay of oscillons during the post-inflationary reheating epoch from inflaton oscillations around asymptotically flat potentials $V(\varphi)$ in the presence of an external coupling of the form $\frac{1}{2}\, g^2\, \varphi^2\, \chi^2$. It is well-known that in the absence of such an external coupling, the attractive self-interaction term in the potential leads to the formation of copious amounts of long-lived oscillons both for symmetric and asymmetric plateau potentials. We perform a detailed numerical analysis to study the formation of oscillons in the α-attractor E- and T-model potentials using the publicly available lattice simulation code $\mathcal{C}$osmo$\mathcal{L}$attice. We observe the formation of nonlinear oscillon-like structures with the average equation of state $\langle w_\varphi \rangle \simeq 0$ for a range of values of the inflaton self-coupling λ and the external coupling g^2. Our results demonstrate that oscillons form even in the presence of an external coupling and we determine the upper bound on g^2 which facilitates oscillon formation. We also find that eventually, these oscillons decay into the scalar inflaton radiation as well as into the quanta of the offspring field χ. Thus, we establish the possibility that reheating could have proceeded through the channel of oscillon decay, along with the usual decay of the oscillating inflaton condensate into χ particles. For a given value of the self-coupling λ, we notice that the lifetime of a population of oscillons decreases with an increase in the strength of the external coupling, following an (approximately) *inverse power-law* dependence on g^2.

Keywords: inflation, physics of the early universe, cosmology of theories beyond the SM

ArXiv ePrint: 2406.00108

https://doi.org/10.1088/1475-7516/2024/10/082

JCAP10(2024)082

Contents

Units, notations and convention

- Einstein's gravity (**GR**) with sign $(-,+,+,+)$
- Natural units $\hbar, c = 1$, reduced Planck mass $m_p = \frac{1}{\sqrt{8\pi G}}$
- Conformal time $\int \mathrm{d}\tau = \int \frac{\mathrm{d}t}{a(t)}$
- Derivative w.r.t. coordinate time $\frac{\mathrm{d}\Upsilon}{\mathrm{d}t} \equiv \dot{\Upsilon}$ and w.r.t. conformal time $\frac{\mathrm{d}\Upsilon}{\mathrm{d}\tau} \equiv \Upsilon'$
- $3d$ vectors are denoted in **boldface**, e.g. the comoving spatial coordinate vector is denoted as $\boldsymbol{x}$, while the comoving momentum is denoted as $\boldsymbol{k}$
- Inflaton field φ, homogeneous inflaton condensate ϕ and inflaton fluctuations $\delta\varphi$

1 Introduction

Cosmic inflation is a rapid accelerated expansion of space in the very early universe which provides natural initial conditions for the hot Big Bang phase [1–6]. In the simplest inflationary scenario, this acceleration is facilitated by a single canonical scalar field φ, called the inflaton field, which slowly rolls down a potential $V(\varphi)$. Scalar quantum fluctuations [6–10] generated

JCAP10(2024)082

during inflation provide the primordial seeds for the formation of structure in the universe, while tensor fluctuations [6, 11–13] constitute a background of stochastic gravitational waves (GWs) in the post-inflationary universe.

Over the past two decades, strong constraints have been imposed on the functional form of the inflaton potential by precision measurements of the anisotropies of the Cosmic Microwave Background (CMB) radiation [14, 15]. The latest CMB observations by the BICEP/Keck collaboration [16], combined with the Planck measurements [15], constrain the ratio of the tensor to scalar power spectra, called the tensor-to-scalar ratio, to be $r \leq 0.036$ on large cosmological scales with 95% confidence. The aforementioned bound on r translates into an upper bound on the Hubble parameter during inflation, thus directly related to its energy scale. Equivalently, the latest CMB observations favour relatively shallow potentials, while ruling out a large number of popular models of inflation [17]. For example, simple monomial potentials of the form $V(\varphi) \propto \varphi^n$ are disfavoured due to their tendency to overproduce primordial gravitational waves [18], whereas those with asymptotically flat plateaus (symmetric or asymmetric) are currently the most favoured models due to their suppressed levels of such primordial gravitational waves [18, 19].

Towards the end of inflation, the slow-roll conditions are violated as the inflaton field begins to descend more rapidly down its potential. After the end of inflation, the inflaton begins to oscillate coherently around the minimum of its potential. The universe transitions to the reheating epoch characterised by the decay of the rapidly oscillating inflaton condensate, and the inflaton eventually transfers most of its energy into the Standard Model particles, marking the beginning of radiation domination. Historically, particle production during reheating was modelled by the slow perturbative decay of massive inflaton particles, eventually leading to the thermalisation of the universe to the radiation-dominated epoch [20, 21]. However, it was later realised that non-perturbative effects usually dominate during the initial regime of reheating due to the coherent nature of the inflaton oscillations [22]. In particular, the phenomenon of *parametric resonance* results in the amplification of perturbations of the inflaton field and other fields coupled to it, resulting in copious particle production [23–29]. In general, reheating is often divided into three distinct regimes — *(i)* a *preheating* phase where the non-perturbative effects lead to an exponential growth of the field fluctuations in distinct resonance bands, *(ii)* a *backreaction* phase where the produced field quanta strongly backreact on the inflaton condensate, thereby quenching the parametric resonance, and *(iii)* the *thermalisation* phase where a cascade of perturbative processes lead to the eventual thermalisation of the universe, thus facilitating the commencement of the hot Big Bang phase.

During preheating in non-linear potentials, the oscillating inflaton condensate drives the amplification of perturbations of the inflaton field itself (aptly called *self-resonance*) and other coupled bosonic fields (called *external resonance*). This leads to the exponential growth of field fluctuations as $e^{\mu_k t}$, where μ_k, known as the Floquet exponent, gives the associated timescale for the rapid growth. Extensive analyses on the subject have been performed in refs. [23–27]. Of particular importance is the formation of dense and localised field configurations that oscillate in time, called *oscillons* [30–39]. Remarkably, formation of oscillons is a prediction of generic real scalar field theories with self-interaction potentials that are shallower than φ^2 around the minimum because such potentials allow the scalar

JCAP10(2024)082

field to feel the effect of the attractive self-interaction as it oscillates about its minimum. Oscillons do not strictly possess a conserved charge, hence they are technically not stable. Nevertheless, due to the fact that they are non-linear configurations, they can be exceptionally long-lived (hence *quasi-stable*), decaying slowly via the emission of radiation [37, 40–42]. By relaxing the reality condition on φ, thereby allowing it to be a complex field, it is possible to form solitonic objects known as *Q-balls*[1] [43–45] which have been studied in the context of supersymmetric dark matter, and more recently as possible sources to explain boson stars and superradiance phenomena therein [46, 47].

Oscillons were extensively studied in condensed matter and nonlinear systems in refs. [48, 49]. In the context of early universe physics, they were initially considered in scenarios of cosmological phase transitions [50–53], while the study of oscillons has more recently been extended to other cosmological phenomenon, ranging from providing the seeds for primordial black holes (PBHs) [54–57], of primordial gravitational waves [35, 58–63] and for the formation of non-linear structure in ultra-light dark matter (ULDM) [64–67]. From the preheating perspective, since the formation of these structures require potentials close to the minimum that are shallower than quadratic in φ, initial analytical and numerical investigations were carried out in theories with an even polynomial potential containing terms up to $\mathcal{O}(\varphi^6)$ of the form $V(\varphi) = m^2\varphi^2/2 - \lambda\,\varphi^4/4 + g\,\varphi^6/6$ [68–70], where *flat-top* oscillons were shown to exist. They have subsequently been studied in axion monodromy potentials [30–32, 71], hilltop potentials [72–74], α-attractor models [34, 36, 39] and in Einstein-Cartan Higgs inflationary model [75]. In ref. [34], for potentials of the form $V(\varphi) \propto \varphi^{2n}$ close to its minimum, the authors used the T-model to quantify the differences between $n = 1$ and $n > 1$ (where the minima are quadratic and non-quadratic respectively at leading order), leading to quite different field configurations as end products. They demonstrated that oscillons can form when $n = 1$ such that the time-averaged equation of state parameter $\langle w_\varphi \rangle \to 0$. In cases where $n > 1$, dense transients form initially which quickly fragment into radiation within a few e-folds with $\langle w_\varphi \rangle \to \frac{1}{3}$. More recently, ref. [39] demonstrated that oscillons can also form in asymmetric potentials by using lattice simulations of the E-model α-attractor potential, obtaining results that are qualitatively similar to those of the T-model.

Most of the oscillon literature has studied their formation by explicitly assuming the absence of alternate decay channels, such as neglecting the coupling of the inflaton to an external field. However, it is important to include such interactions and couplings since the universe needs to be reheated to a thermal plasma state before the commencement of Big Bang Nucleosynthesis (BBN). In principle, the inflaton can have couplings to both fermionic and bosonic degrees of freedom. However, the phenomenon of parametric resonance is only applicable to the production of bosons, due to Bose enhancement effects. Furthermore, most UV complete theories of inflation, such as those arising from string compactifications, predict the existence of multiple scalar fields (*moduli fields*) [76–78] along with the inflaton. Hence, it is natural to expect the inflaton to be coupled to one or more scalar degrees of freedom.

In this paper, we consider such a case where the inflaton field φ is coupled to a light scalar field χ, which we call the *offspring field*. We carry out detailed (3+1)-dimensional

[1] Q-balls have a conserved charge in the particle number associated with a global U(1) symmetry. An approximate conserved charge is often defined for oscillons in analogy with Q-balls.

JCAP10(2024)082

lattice simulations of the inflaton dynamics in the E- and T-model α-attractor potentials with a quadratic-quadratic external coupling to χ of the simplest form $\mathcal{L}_{\rm int} \supset \frac{1}{2}\, g^2\, \varphi^2 \chi^2$. By considering a range of possible values of the coupling parameter g^2, we carry out a thorough numerical investigation of inflaton decay with the primary objective of quantifying the conditions for the formation and decay of oscillons. The presence of the two coupling parameters, namely the self-coupling λ appearing in the inflaton potential (which determines the tensor-to-scalar ratio during inflation), and the external coupling g^2, allows us to determine the subspace of the parameter space, $\{\lambda,\, g^2\}$, leading to oscillon formation as well as to study their subsequent decay due to the presence of such simple external interactions; all the while ensuring that the inflationary predictions are consistent with the latest CMB constraints [15, 16, 18]. Consequently, we establish an upper bound on the external coupling g^2 for which oscillons form for a given value of the self-coupling λ, both for the E- and the T-model potentials. Furthermore, in reference to the decay of oscillons, we establish the novel possibility of a substantial production of the offspring particles during preheating to have arisen via oscillon decay, in addition to the usual channel of inflaton condensate decay. We observe that the lifetime of a population of oscillons decreases with the increase in the strength of the external coupling, following an (approximately) inverse power-law dependence on g^2. Our upcoming paper [79] will be dedicated to an analytical treatment of oscillon formation and decay in asymptotically flat potentials in the presence of such an external coupling.

This paper is organized as follows: in section 2, after providing a brief introduction to the scalar field dynamics during inflation, we set up the complete set of coupled field equations describing the expansion of space and the decay of the inflaton in the post-inflationary epoch. We introduce both E- and T-model α-attractors as representatives for asymptotically flat potentials of symmetric and asymmetric types, respectively. In section 3, a Floquet analysis is carried out to characterize the inflaton decay via self and external parametric resonances in the linear regime where we generate the instability chart for the quanta of the decay modes during the preheating phase in order to demonstrate the existence of a broad-band resonance region followed by multiple narrow ones. In section 4 we carry out full $(3+1)d$ lattice simulations for the E- and T-model potentials and confirm the formation of oscillons for a subspace of the parameter space $\{\lambda,\, g^2\}$. We also study the lifetime of oscillons due to their decay via scalar inflaton radiation as well as into the quanta of the offspring field. We conclude in section 5 with a discussion of the primary inferences of this work, and its possible future extension, especially in the context of analytical treatment of the oscillon lifetime. Various appendices provide supplementary information on the inflationary and post-inflationary scalar field dynamics of asymptotically flat potentials.

2 Dynamics of the post-inflationary epoch

2.1 Scalar field dynamics during inflation

In the simplest inflationary scenario which we consider in this work, the quasi-exponential expansion of space is sourced by a single canonical scalar field called the *inflaton* $\varphi(t, \boldsymbol{x})$ with a potential $V(\varphi)$ which is minimally coupled to gravity. In this standard paradigm, inflaton couplings to the external fields are assumed to be very weak, so that they can be

JCAP10(2024)082

neglected during inflation, ensuring that the dynamics is completely dictated by the inflaton field. Hence, during inflation, the system is described by the action

$$S[g_{\mu\nu},\varphi] = \int \mathrm{d}^4x\,\sqrt{-g}\left(\frac{m_p^2}{2}\,R - \frac{1}{2}\,\partial_\mu\varphi\,\partial_\nu\varphi\,g^{\mu\nu} - V(\varphi)\right). \tag{2.1}$$

In linear perturbation theory during inflation, we split the metric and the inflaton field into their corresponding background and fluctuations, namely

$$g_{\mu\nu}(t,\boldsymbol{x}) = \bar{g}_{\mu\nu}(t) + \delta g_{\mu\nu}(t,\boldsymbol{x})\,; \quad \varphi(t,\boldsymbol{x}) = \phi(t) + \delta\varphi(t,\boldsymbol{x})\,.$$

The perturbed line element in the ADM formalism [80, 81] can be written as

$$\mathrm{d}s^2 = -\alpha^2\,\mathrm{d}t^2 + \gamma_{ij}\Big(\mathrm{d}x^i + \beta^i\,\mathrm{d}t\Big)\Big(\mathrm{d}x^j + \beta^j\,\mathrm{d}t\Big)\,, \tag{2.2}$$

where the non-dynamical Lagrange multipliers, $\alpha = 1 + \delta\alpha$ and β^i, are the lapse and shift functions respectively, which are completely fixed by the Hamiltonian and momentum constraints, while γ_{ij} are the true dynamical metric perturbations. During inflation, it is convenient to work in the *comoving gauge*[2] where the inflaton and metric fluctuations are given by [6, 81, 82]

$$\delta\varphi(t,\boldsymbol{x}) = 0\,; \quad \gamma_{ij}(t,\boldsymbol{x}) = a^2\left[\left(1 + 2\,\zeta(t,\boldsymbol{x})\right)\delta_{ij} + h_{ij}(t,\boldsymbol{x})\right], \tag{2.3}$$

where $\zeta(t,\boldsymbol{x})$ and $h_{ij}(t,\boldsymbol{x})$ are the gauge-invariant comoving curvature perturbation (scalar-type), and transverse and traceless perturbations (tensor-type), respectively. The scalar perturbations eventually induce density and temperature fluctuations in the hot Big Bang phase, which subsequently facilitates the formation of the large-scale structure in the universe. Meanwhile, the tensor fluctuations propagate as gravitational waves (GWs) which, at late times, constitute a stochastic background of GWs.

The perturbed action in the comoving gauge during inflation can be expressed as [82]

$$S[g_{\mu\nu},\varphi] = S_B[\bar{g}_{\mu\nu},\phi] + S^{(2)}[\zeta] + S^{(2)}[h_{ij}] + S_{\rm int}[\zeta,h_{ij}]\,, \tag{2.4}$$

where $S_B[\bar{g}_{\mu\nu},\phi]$ is the background action, while $S^{(2)}[\zeta]$, $S^{(2)}[h_{ij}]$ are the quadratic actions for the scalar and tensor fluctuations (which results in linear field equations for the fluctuations). The term $S_{\rm int}[\zeta,h_{ij}]$ is the action for fluctuations beyond the linear order which leads to primordial non-Gaussianity (detailed discussions on this topic can be found in refs. [6, 81, 82]).

For the background evolution of $\{\bar{g}_{\mu\nu},\phi\}$ during inflation, specializing to a spatially flat FLRW metric and the homogeneous part ϕ of the scalar field φ, one gets

$$\mathrm{d}s^2 = -\mathrm{d}t^2 + a^2(t)\left[\mathrm{d}x^2 + \mathrm{d}y^2 + \mathrm{d}z^2\right], \tag{2.5}$$

$$T^\mu{}_\nu \equiv \mathrm{diag}\Big(-\rho_\phi,\, p_\phi,\, p_\phi,\, p_\phi\Big)\,, \tag{2.6}$$

[2]Note that we do not work in the comoving gauge while describing the post-inflationary dynamics in section 2.2. In fact, the metric perturbations can be safely ignored while studying the preheating dynamics which occurs over shorter time scales and on small scales $k > aH$.

JCAP10(2024)082

where the energy density $\rho_{_\phi}$, and pressure $p_{_\phi}$, of the homogeneous inflaton condensate are given by

$$\rho_{_\phi} = \frac{1}{2}\dot{\phi}^2 + V(\phi)\,; \quad p_{_\phi} = \frac{1}{2}\dot{\phi}^2 - V(\phi)\,. \tag{2.7}$$

Evolution of the scale factor $a(t)$ is governed by the Friedmann equations

$$H^2 = \frac{1}{3m_p^2}\,\rho_\phi = \frac{1}{3m_p^2}\left[\frac{1}{2}\dot{\phi}^2 + V(\phi)\right], \tag{2.8}$$

$$\dot{H} \equiv \frac{\ddot{a}}{a} - H^2 = -\frac{1}{2m_p^2}\,\dot{\phi}^2\,, \tag{2.9}$$

while ϕ satisfies the equation of motion

$$\ddot{\phi} + 3\,H\dot{\phi} + V_{,\phi} = 0\,, \tag{2.10}$$

where $V_{,\phi} \equiv \mathrm{d}V/\mathrm{d}\phi$. Evolution of various physical quantities during inflation is usually described with respect to the number of e-folds of expansion which is defined by $N = \ln(a/a_i)$, where a_i is the scale factor at some arbitrary epoch at very early times during inflation. A better physical quantity that quantifies the extent of inflation is the *number of e-folds before the end of inflation*, which is defined as

$$N_e(a) = \ln\left(\frac{a_e}{a}\right) = \int_t^{t_e} H(t)\,\mathrm{d}t, \tag{2.11}$$

where $H(t)$ is the Hubble parameter during inflation. Note that a_e denotes the scale factor at the end of inflation, hence $N_e = 0$ corresponds to the end of inflation. Typically a period of quasi-de Sitter (exponential) inflation lasting for at least 60–70 e-folds is required in order to address the problems of the standard hot Big Bang model. We denote $N_\star$ as the number of e-folds (before the end of inflation) when the CMB pivot scale

$$k_\star = (aH)_\star = 0.05\,\mathrm{Mpc}^{-1} \tag{2.12}$$

left the comoving Hubble radius during inflation. Typically $N_\star \in [50, 60]$ depending on the details of reheating after inflation (see refs. [83, 84]). In this work, we fix $N_\star = 60$.

Background kinematics during inflation is usually characterised by the first two Hubble slow-roll parameters ϵ_H, η_H, defined as [6, 85]

$$\epsilon_H = -\frac{\dot{H}}{H^2} = -\frac{\mathrm{d}\ln H}{\mathrm{d}N} = \frac{1}{2m_p^2}\,\frac{\dot{\phi}^2}{H^2}\,, \tag{2.13}$$

$$\eta_H = -\frac{\ddot{\phi}}{H\dot{\phi}} = \epsilon_H - \frac{1}{2\epsilon_H}\,\frac{\mathrm{d}\epsilon_H}{\mathrm{d}N}\,. \tag{2.14}$$

For asymptotically flat potentials, there exists a slow-roll regime of inflation (ensured by the presence of the Hubble friction term [86, 87] in eq. (2.10)), defined by

$$\epsilon_H,\ |\eta_H| \ll 1\,. \tag{2.15}$$

JCAP10(2024)082

Using the definition of the Hubble parameter, $H = \dot{a}/a$, we have $\ddot{a}/a = \dot{H} + H^2 = H^2(1 + \dot{H}/H^2)$. From the expression for ϵ_H in eq. (2.13), it is easy to see that

$$\frac{\ddot{a}}{a} = H^2 \left(1 - \epsilon_H\right), \tag{2.16}$$

which implies that the universe accelerates, $\ddot{a} > 0$, when $\epsilon_H < 1$. Using eq. (2.8), the expression for ϵ_H in eq. (2.13) reduces to $\epsilon_H \simeq \frac{3}{2}\frac{\dot{\phi}^2}{V}$ when $\dot{\phi}^2 \ll V$. In fact, under the slow-roll conditions in eq. (2.15), the Friedmann eqs. (2.8) and (2.10) take the form

$$H^2 \simeq \frac{1}{3m_p^2} V(\phi)\,; \quad \dot{\phi} \simeq -\frac{V_{,\phi}}{3H}\,. \tag{2.17}$$

For asymptotically flat potentials the power spectra of scalar and tensor perturbations generated *via* vacuum quantum fluctuations during slow-roll inflation agree well with the latest CMB observations [15, 16] as discussed in appendix A. The end of inflation is marked by the violation of slow roll, with $\epsilon_H = 1$, which corresponds to $\dot{\phi}^2_{\rm end} = V(\phi_{\rm end})$ as can be inferred from eqs. (2.13) and (2.16). After the end of inflation, the homogeneous inflaton condensate begins to oscillate around the minimum of its potential.

2.2 Dynamics of the post-inflationary universe

The inflationary paradigm is formulated to naturally facilitate the transition into the radiation-dominated hot Big Bang phase during the post-inflationary epoch. The key element of this transient reheating phase, is the ability of the inflaton field φ to decay to other fields after the end of inflation, thereby providing a natural mechanism to transfer the energy stored in the universe with φ to the other fields which eventually thermalise, thereby providing the radiation dominated era we associate with the hot Big Bang phase. With this in mind we focus on one of the simplest incarnations of this decay, where φ is coupled to a massless scalar field χ via an interaction term $\mathcal{I}(\varphi, \chi)$. The system is described by the action

$$S[g_{\mu\nu},\ \varphi,\ \chi] = \int \mathrm{d}^4x\ \sqrt{-g}\left[\frac{m_p^2}{2}\,R - \frac{1}{2}\,\partial_\mu\varphi\,\partial_\nu\varphi\,g^{\mu\nu} - \frac{1}{2}\,\partial_\mu\chi\,\partial_\nu\chi\,g^{\mu\nu} - V(\varphi) - \mathcal{I}(\varphi,\chi)\right]. \tag{2.18}$$

The corresponding field equations are,

$$\ddot{\varphi} + 3\,H\,\dot{\varphi} - \frac{\boldsymbol{\nabla}^2}{a^2}\varphi + V_{,\varphi} + \mathcal{I}_{,\varphi} = 0\,, \tag{2.19}$$

$$\ddot{\chi} + 3\,H\,\dot{\chi} - \frac{\boldsymbol{\nabla}^2}{a^2}\chi + \mathcal{I}_{,\chi} = 0 \tag{2.20}$$

with the Friedmann constraint

$$H^2 = \frac{1}{3\,m_p^2}\left[\left(\frac{1}{2}\,\dot{\boldsymbol{\varphi}}^2 + \frac{1}{2}\,\frac{\boldsymbol{\nabla}\varphi}{a}\cdot\frac{\boldsymbol{\nabla}\varphi}{a} + \boldsymbol{V(\varphi)}\right) + \left(\frac{1}{2}\,\dot{\boldsymbol{\chi}}^2 + \frac{1}{2}\,\frac{\boldsymbol{\nabla}\boldsymbol{\chi}}{\boldsymbol{a}}\cdot\frac{\boldsymbol{\nabla}\boldsymbol{\chi}}{\boldsymbol{a}}\right) + \boldsymbol{\mathcal{I}(\varphi,\,\chi)}\right]. \tag{2.21}$$

The massless offspring field χ is assumed to behave as a spectator/test field during inflation which contributes negligibly to the total energy density and couples very weakly to the inflaton. Since the accelerated expansion during inflation rapidly dilutes the quanta of the χ field, we can assume χ to be in its vacuum state at the end of inflation.

JCAP10(2024)082

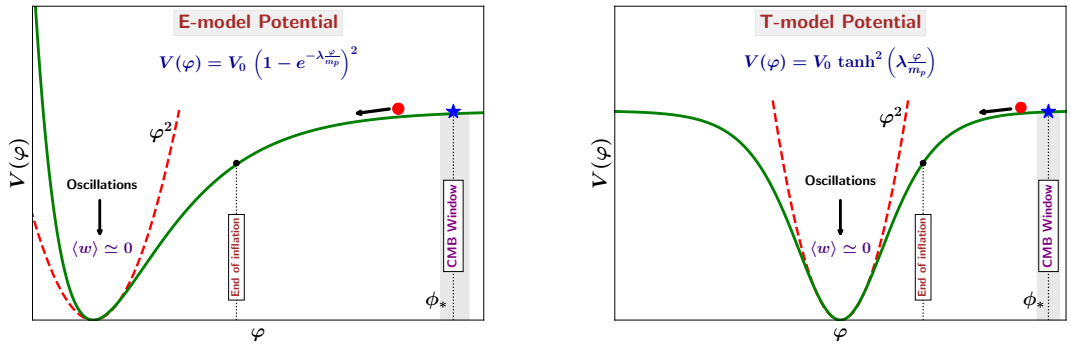

(a) (b)

Figure 1. This figure schematically depicts asymptotically flat inflationary plateau potentials. The *left panel* shows an asymmetric potential featuring only a single plateau-like wing (E-model α-attractor) which supports slow-roll inflation. While the *right panel* shows a symmetric potential possessing two plateau-like wings (T-model α-attractor), both of which can support slow-roll inflation. During the post-inflationary oscillations, the attractive non-linear self-interactions result in the fragmentation of the oscillating inflaton condensate to form oscillons.

As mentioned in section 1, we will be focusing on the formation and lifetime of oscillons in both the asymmetric E-model and the symmetric T-model α-attractor potentials, which are shown in figure 1 [88, 89], using parameters of the models which are consistent with CMB observations [14, 15]. In particular we consider the E-model potential of the form

$$V(\varphi) = V_0 \left[1 - e^{-\lambda_{\rm E} \frac{\varphi}{m_p}}\right]^2 ; \tag{2.22}$$

or, the T-model potential of the form,

$$V(\varphi) = V_0 \tanh^2\left(\lambda_{\rm T} \frac{\varphi}{m_p}\right) , \tag{2.23}$$

with a *quadratic-quadratic coupling* to the offspring field χ of the form

$$\mathcal{I}(\varphi, \chi) = \frac{1}{2} g^2 \varphi^2 \chi^2 . \tag{2.24}$$

Given the forms of $V(\varphi)$ and $\mathcal{I}(\varphi, \chi)$, it follows that the post-inflationary dynamics of the system is primarily dictated by the strength of the parameters λ and g^2. Taking the importance of non-linear and non-thermal processes into account, the reheating dynamics can in general be divided into three distinct phases [25, 26, 90] as described below.

2.2.1 Preheating

As inflation ends with the breakdown of slow-roll, the (almost) homogeneous inflaton condensate ϕ rolls down the potential $V(\phi)$ and begins to oscillate about its minimum. In the presence of couplings, both self and external, the fluctuations of φ and χ are enhanced via *parametric*

JCAP10(2024)082

resonance. In particular, using $f_k(t)$ to represent the Fourier modes of the fluctuations of either φ or χ, it satisfies the equation of a damped parametric oscillator of the form

$$\ddot{f}_k(t) + 3H\,\dot{f}_k(t) + \Omega_k^2(t)\,f_k(t) = 0\,; \quad \text{with} \quad \Omega_k(t+T_k) \simeq \Omega_k(t)\,, \tag{2.25}$$

where T_k is the periodicity of the parametric frequency $\Omega_k(t)$ [26, 27, 91, 92]. During the coherent oscillations of the inflaton, it is possible for $\Omega_k(t)$ to change *non-adiabatically* for certain ranges of k values, namely,

$$\left|\frac{\dot{\Omega}_k(t)}{\Omega_k^2(t)}\right| \geq 1\,, \tag{2.26}$$

thereby enabling efficient parametric resonance to occur during preheating which in turn results in the explosive (non-thermal) particle production in discrete bands of the comoving wavenumber k of the quanta of the field fluctuations [26]. As a result, the energy contained in the oscillating condensate $\phi(t)$ is rapidly transferred to the fluctuations of φ and χ. The precise nature of the periodicity relies on the functional form of the inflaton self-interaction potential, $V(\varphi)$, and that of the external coupling, $\mathcal{I}(\varphi,\,\chi)$. In section 3, we use the approach of Floquet theory to analyse the nature of the growth of these fluctuations at the linear level for the potentials and interaction terms given by eqs. (2.22)–(2.24).

2.2.2 Backreaction and termination of resonance

The second phase of reheating can proceed along two different routes. The first occurs if the resonance is sufficiently strong and constitutes a significant backreaction of the resonantly produced field quanta of φ and χ on the homogeneous inflaton condensate $\phi(t)$. The presence of newly produced field quanta may change the effective mass of the oscillating inflaton. Moreover, when the energy densities of the fluctuations become comparable to that of the condensate, backreaction terminates the resonant production of the field quanta mentioned in section 2.2.1, thereby quenching the growth of the fluctuations [25, 26]. However, if the resonance is not strong enough (i.e. if fluctuations of φ and χ remain small), then the second route is followed, namely the preheating phase terminates because of the redshifting of the physical momenta $k_p = k/a$ (due to the expansion of the background space), in the absence of significant backreaction.

2.2.3 Thermalisation

In the third and final phase, the remaining inflaton condensate $\phi(t)$ decays perturbatively, leading to a large number of decay products. This in turn leads to the fluctuations of φ and χ re-scattering off these new decay products and further decaying into the quanta of other fields that they are (very weakly) coupled to. Eventually the decay products thermalise resulting in the commencement of the familiar radiation-dominated hot Big Bang phase.

In sections 3 and 4, we analyse in detail the first two phases of reheating: preheating and backreaction, from both a linear point of view (using linear Floquet theory) and a fully non-linear numerical perspective, in the latter case via detailed $3d$ lattice simulations using $\mathcal{C}$osmo$\mathcal{L}$attice [93, 94].

JCAP10(2024)082

3 Linear parametric resonance and Floquet theory

A convenient way to characterise the dynamics during the early stages of preheating is to linearize the field fluctuations in eqs. (2.19) and (2.20) and carry out the standard Floquet analysis [26, 95–98]. To begin with, we split each of the field contents in the eqs. (2.19)–(2.21) into a homogeneous background and small fluctuations around that background, namely

$$\varphi(t, \boldsymbol{x}) = \phi(t) + \delta\varphi(t, \boldsymbol{x})\,; \tag{3.1}$$

$$\chi(t, \boldsymbol{x}) = \bar{\chi}(t) + \delta\chi(t, \boldsymbol{x})\,. \tag{3.2}$$

As discussed in section 2.2, since the χ field is expected to be in its vacuum state at the end of inflation, we have $\bar{\chi}(t) \simeq 0$, leading to $\delta\chi(t, \boldsymbol{x}) = \chi(t, \boldsymbol{x})$. From hereon, we will simply denote the fluctuations $\delta\chi$ as χ. Using eqs. (2.19) and (2.20), one can arrive at equations of the form of eq. (2.25) by making the following approximations to retain only terms that are linear in the fluctuations $\delta\varphi$, χ.

1. The energy density of the system is predominantly contained in the homogeneous inflaton condensate $\phi(t)$, i.e.

   $$\phi_0(t) \gg |\delta\varphi(t, \boldsymbol{x})|,\, |\chi(t, \boldsymbol{x})|\,;$$

   and

   $$\rho_\phi \gg \rho_\chi,\, \rho_{\delta\varphi}\,,$$

   where $\phi_0(t)$ is the amplitude of oscillations of the inflaton.

2. Since $\bar{\chi}(t) = 0$, the interaction term $\mathcal{I}(\varphi, \chi)$ given in eq. (2.24) becomes

   $$\mathcal{I}(\varphi, \chi) = \mathcal{I}(\phi + \delta\varphi, \chi) \simeq \frac{1}{2}\, g^2\, \phi^2(t)\, \chi^2\,,$$

   which can be dropped from the Friedmann constraint eq. (2.21) at linear order. Furthermore, we get

   $$\mathcal{I}_{,\varphi} \equiv g^2\, \varphi\, \chi^2 = g^2\, (\phi(t) + \delta\varphi)\, \chi^2 \simeq g^2\, \phi(t)\, \chi^2\,,$$

   which can be dropped from the evolution eq. (2.19) at linear order. Similarly, the last term of the left hand side of eq. (2.20) becomes

   $$\mathcal{I}_{,\chi} \equiv g^2\, \varphi^2\, \chi = g^2\, (\phi(t) + \delta\varphi)^2\, \chi \simeq g^2\, \phi^2(t)\, \chi$$

   at linear order.

3. Under the linear approximation, the inflaton potential becomes

   $$V(\varphi) = V(\phi + \delta\varphi) \simeq V(\phi) + V_{,\phi}(\phi)\, \delta\varphi$$

   and its derivative becomes

   $$V_{,\varphi}(\varphi) = V_{,\varphi}(\phi + \delta\varphi) \simeq V_{,\phi}(\phi) + V_{,\phi\phi}(\phi)\, \delta\varphi\,.$$

JCAP10(2024)082

We again stress that these approximations are valid during the early stages of preheating, before backreactions from $\delta\varphi$ and χ become significant, i.e. $\rho_{\delta\varphi}, \rho_\chi \sim \rho_\phi$, as discussed in section 2.2.2. Under the aforementioned approximations, the field eqs. (2.19) and (2.20) reduce to

$$\ddot{\phi} + 3H\dot{\phi} + V_{,\phi} = 0\,, \tag{3.3}$$

$$\ddot{\delta\varphi} + 3H\dot{\delta\varphi} + \left[-\frac{\boldsymbol{\nabla}^2}{a^2} + V_{,\phi\phi}(\phi)\right]\delta\varphi = 0\,, \tag{3.4}$$

$$\ddot{\chi} + 3H\dot{\chi} + \left[-\frac{\boldsymbol{\nabla}^2}{a^2} + g^2\,\phi^2\right]\chi = 0\,, \tag{3.5}$$

and the Friedmann eq. (2.21) becomes

$$H^2 = \frac{1}{3\,m_p^2}\left[\frac{1}{2}\,\dot{\phi}^2 + V(\phi)\right]. \tag{3.6}$$

Note that in eqs. (3.3) and (3.6) we have dropped the $\delta\varphi$ terms in order to describe the background dynamics in terms of the purely homogeneous condensate at the end of inflation. Hence, they represent the background equations, with respect to which fluctuations are defined. The corresponding equations for the evolution of the Fourier modes $\delta\varphi_k$ and χ_k, take the following form

$$\ddot{\delta\varphi}_k + 3H\dot{\delta\varphi}_k + \left[\frac{k^2}{a^2} + V_{,\phi\phi}(\phi)\right]\delta\varphi_k = 0\,; \tag{3.7}$$

$$\ddot{\chi}_k + 3H\dot{\chi}_k + \left[\frac{k^2}{a^2} + g^2\,\phi^2\right]\chi_k = 0\,. \tag{3.8}$$

Eqs. (3.7) and (3.8) describe two independent parametric oscillators with time-dependent damping terms $3H\dot{\delta\varphi}_k$ and $3H\dot{\chi}_k$ and parametric frequencies of the form

$$\Omega^2_{k,\delta\varphi}(t) = \frac{k^2}{a^2} + V_{,\phi\phi}(\phi)\,; \quad \Omega^2_{k,\chi}(t) = \frac{k^2}{a^2} + g^2\,\phi^2(t)\,. \tag{3.9}$$

According to Floquet theory [95–98], the solutions to eqs. (3.7) and (3.8) (which generally have to be obtained numerically) are of the form,

$$\delta\varphi_k(t) = \mathcal{P}_+(t)\,e^{\mu_k t} + \mathcal{P}_-(t)\,e^{-\mu_k t}\,, \tag{3.10}$$

$$\chi_k(t) = \mathcal{Q}_+(t)\,e^{\nu_k t} + \mathcal{Q}_-(t)\,e^{-\nu_k t} \tag{3.11}$$

where μ_k, ν_k are the corresponding *Floquet exponents* and $\mathcal{P}_\pm(t)$, $\mathcal{Q}_\pm(t)$ are periodic functions with the same oscillation period as that of the background field. Floquet exponents are complex in general and those modes with $\Re(\mu_k)$, $\Re(\nu_k) \neq 0$ experience resonant growth with time, whereas for $\Re(\mu_k)$, $\Re(\nu_k) = 0$, the corresponding modes are oscillatory. One can map such regions onto a *Floquet chart* as shown in figure 2, and further analyse the nature of the resonance (either narrow or broad) as a function of the oscillation amplitude and Fourier mode k (see figure 3). Figures 2 and 3 are obtained numerically by solving eqs. (3.7) and (3.8) ignoring the expansion of space by setting $H = 0$ and setting $a = 1$.

JCAP10(2024)082

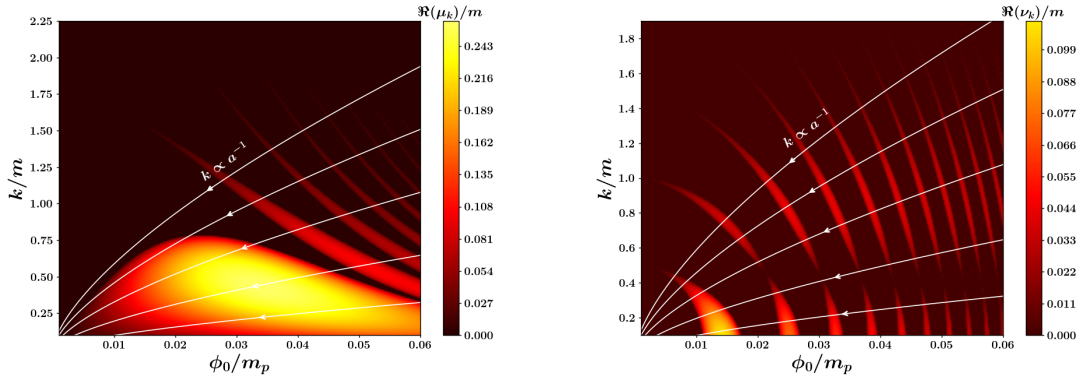

Figure 2. The Floquet charts exhibiting the instability bands corresponding to the inflaton decay *via* self-resonance (*left*) in the T-model with $\lambda_{\rm T} = 50\sqrt{2/3}$ and external resonance (*right*) with $g^2 = 8 \times 10^{-6}$ are shown, obtained by numerically solving eqs. (3.7) and (3.8) ignoring the expansion of the background space, i.e., setting $H = 0$ and $a = 1$. The darker regions correspond to stable solutions with $\{\Re(\mu_k), \Re(\nu_k)\} \to 0$, while the brighter regions correspond to resonance (instability) bands where $\delta\varphi_k$, χ_k grow exponentially, namely $\delta\varphi_k \propto e^{\Re(\mu_k)t}$, $\chi_k \propto e^{\Re(\nu_k)t}$. The white flow curves display the passage of the system through multiple resonance bands due to the expansion of the background space on longer time scales. The expansion of space reduces the amplitude of oscillations $\phi_0(t)$, and results in the redshifting of the physical momenta $k_p = k/a$.

The brighter (or shaded regions) correspond to resonance bands where $\delta\varphi_k$, χ_k experience exponential growth i.e. $\delta\varphi_k(t) \propto e^{\Re(\mu_k)t}$, $\chi_k(t) \propto e^{\Re(\nu_k)t}$. Since the timescale of expansion of the background space is much longer compared to that of the ϕ-oscillations, its effect on the parameters, namely the redshifting of physical momenta $k_p = k/a$ and the decrease in the amplitude of oscillations ϕ_0, can simply be represented by white flow curves through the resonance bands, as shown in figure 2.

As is clear from the evolution equations in eqs. (3.3) and (3.6), making progress at the analytic level, even for the background evolution of $H(t)$ and $\phi(t)$ requires us to be able to handle the non-linear functional form of the potential $V(\varphi)$. In many cases, including the two potentials we are concentrating on, eqs. (2.22) and (2.23), the functional form of $V(\varphi)$ is often quite complicated. However, we can still make progress by recalling that reheating in general takes place for small-amplitude regimes, where $\phi_0 \ll m_p$, in which case we can Taylor expand the potentials, leading to

$$V(\varphi)\big|_{\text{E-model}} \simeq \frac{1}{2}\left(2\lambda_{\rm E}^2\frac{V_0}{m_p^2}\right)\varphi^2 - \frac{1}{3}\left(3\lambda_{\rm E}^3\frac{V_0}{m_p^3}\right)\varphi^3 + \frac{1}{4}\left(\frac{7}{3}\lambda_{\rm E}^4\frac{V_0}{m_p^4}\right)\varphi^4 + \dots\,, \tag{3.12}$$

$$V(\varphi)\big|_{\text{T-model}} \simeq \frac{1}{2}\left(2\lambda_{\rm T}^2\frac{V_0}{m_p^2}\right)\varphi^2 - \frac{1}{4}\left(\frac{8}{3}\lambda_{\rm T}^4\frac{V_0}{m_p^4}\right)\varphi^4 + \dots \tag{3.13}$$

respectively. This allows us to evaluate the time-averaged equation of state (ignoring $\mathcal{O}(\varphi^3)$ and higher terms) yielding $\langle w_\varphi\rangle = \frac{n-1}{n+1}$, for $V(\varphi) \sim \varphi^{2n}$, and consequently, the time-averaged expansion of the background space — namely $a \sim t^p$, with $p = \frac{2}{3(1+\langle w_\phi\rangle)}$ (refer to appendix B). From eqs. (3.12) and (3.13), it is easy to see that the mass of the inflaton

JCAP10(2024)082

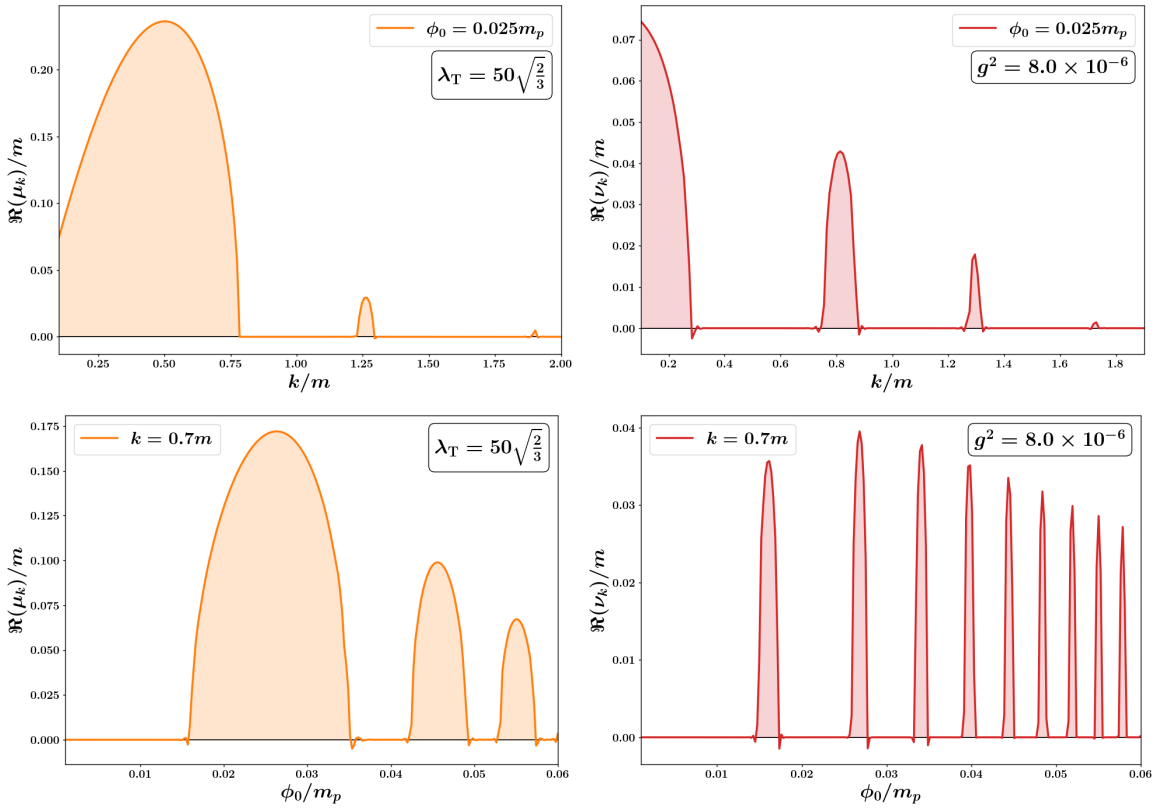

Figure 3. Variations of the (real part of the) Floquet exponents, $\Re(\mu_k)$ (orange), $\Re(\nu_k)$ (red), as a function of the comoving momenta k for a fixed amplitude ϕ_0 (*top row*), and as a function of ϕ_0 for a fixed k (*bottom row*) corresponding to self-resonance (*left*) and external resonance (*right*) in the T-model are shown here. Fluctuations $\delta\varphi_k$, χ_k experience resonant growth when $\Re(\mu_k)$, $\Re(\nu_k) > 0$ (shaded regions).

is related to V_0 and λ as

$$m^2 = 2\,\lambda^2\,\frac{V_0}{m_p^2}\,, \tag{3.14}$$

where $\lambda = \lambda_{\rm E}, \lambda_{\rm T}$ for the E- and the T-models respectively.

It is worth noting that for a range of values of the parameter λ (denoted as $\lambda_{\rm T}$ for the T-model and $\lambda_{\rm E}$ for the E-model), the first few oscillation of $\phi(t)$ about the minimum of the potential correspond to tachyonic regimes. Some details on tachyonic oscillations can be found in appendix C. As the inflaton evolves down its potential, since the amplitude of oscillations $\phi_0(t)$ decreases due to particle production (and due to expansion of the background space), the φ^2 term eventually becomes dominant in eqs. (3.12) and (3.13) leading to Mathieu-like resonance. When this occurs, the structure of the resonance bands for self-resonance changes from the one shown in figure 2 to that corresponding to the Mathieu equation. We do not plot the Floquet-chart for the Mathieu equation here, as these are well known in the literature [23, 29, 99]. Hence, the Floquet chart corresponding to self-resonance in figure 2 is valid only for the first few ϕ-oscillations.

JCAP10(2024)082

Since our primary goal is to study the formation of oscillons, it is important to make the definition of oscillons clear. Oscillons are highly *non-linear* and *non-relativistic* localised field configurations where the spatial gradient (Laplacian) of the field profile is balanced by the field-derivative of the non-linear self-interaction potential. Therefore, both the attractive self-interaction and the gradient terms play a crucial role in their field profile and energy density. In particular, their formation during preheating necessarily requires a dynamical mechanism to facilitate the fragmentation of the homogeneous inflaton condensate, which can then clump together via attractive self-interaction to form oscillons. In summary, the possibility of oscillon formation during preheating requires two *necessary* conditions: (*i*) the presence of an attractive non-linear self-interaction term in the potential i.e. $V(\varphi) = \frac{1}{2}m^2\varphi^2 - |U(\varphi)|$, and (*ii*) an exponential growth of the inflaton inhomogeneities $\delta\varphi_k$ *via* broad parametric resonance. Eqs. (3.12) and (3.13) show that in the small-amplitude regime the potentials contain the desired attractive self-interaction terms suitable for scalar field fragmentation, and oscillon formation, which can be seen from figure 1. Our analysis in this section, as plotted in figures 2 and 3, demonstrates that the second condition is also easily satisfied in the linear regime for a range of values of $\{\phi_0,\, k\}$, even in the presence of an external coupling.

Nevertheless, it is important to remember that while the aforementioned conditions are necessary for oscillon formation, they are not sufficient. If the resonant growth of the inflaton and χ fluctuations continues for long enough, then the energy densities of the fluctuations eventually become comparable to that of the homogeneous condensate and our linear treatment based on parametric resonance breaks down. In general, the growing fluctuations are expected to backreact on the oscillating condensate and break it into inflaton fragments, which can then clump together due to the non-linear self-interaction to form oscillons. Since oscillons are necessarily non-linear field configurations, in order to firmly establish the formation (and later, the lifetime) of oscillons, one needs to carry out detailed numerical lattice simulations in order to capture the non-perturbative dynamics.

In fact, lattice simulations carried out in refs. [39] and [34] show that oscillons do form during the inflaton oscillations around the E- and the T-model potentials, in the absence of any external coupling. However, the question of oscillon formation in the presence of a coupled offspring field has not been investigated systematically in the current literature, which is the primary focus of this work. In section 4, we carry out detailed numerical lattice simulations of the non-linear field eqs. (2.19)–(2.21) in the presence of the external coupling (2.24) as discussed below.

4 Non-linear dynamics: lattice simulations

4.1 CosmoLattice setup and parameters

For the 3*d* lattice simulations of the field equations, we use the publicly available lattice code CosmoLattice [93, 94]. In order to carry out numerical simulations conveniently, we define the following dimensionless variables,

$$\tilde{t} = m\,t\,; \quad \tilde{x} = m\,x\,; \quad \tilde{f} = \frac{1}{\beta}\,\frac{f}{m_p}\,, \tag{4.1}$$

JCAP10(2024)082

where $f = \{\varphi,\ \chi\}$, $m^2 = \frac{2\,V_0\lambda^2}{m_p^2}$ from eq. (3.14), and $\beta \in \mathbb{R}^+$ is a parameter that we have introduced for numerical convenience. In general β should be of the order $\phi_{\rm end}/m_p$, where recall that $\phi_{\rm end}$ marks the end of inflation. In our lattice simulations, we fix $\beta = 10$ throughout. In terms of these variables, we convert the kinetic (K), the gradient (G), the potential (V) and the interaction ($\mathcal{I}$) terms in the action in eq. (2.18) to their corresponding dimensionless counterparts by dividing each term with $\beta^2 m^2 m_p^2$ as follows-

$$\widetilde{F}(\tilde{f}) = \left(\frac{1}{\beta}\,\frac{m_p}{m}\right)^2 \frac{F(f)}{m_p^4}\,, \tag{4.2}$$

where $F = \{K,\ G,\ V,\ \mathcal{I}\}$ (and $f = \{\varphi,\ \chi\}$). As a result, the kinetic and gradient terms in eq. (2.18) become,

$$\widetilde{K}_{\tilde{\varphi}} = \frac{1}{2}\left(\frac{\partial\tilde{\varphi}}{\partial\tilde{t}}\right)^2, \qquad \widetilde{G}_{\tilde{\varphi}} = \frac{1}{2}\frac{1}{a^2(\tilde{t})}\left[\left(\frac{\partial\tilde{\varphi}}{\partial\tilde{x}}\right)^2 + \left(\frac{\partial\tilde{\varphi}}{\partial\tilde{y}}\right)^2 + \left(\frac{\partial\tilde{\varphi}}{\partial\tilde{z}}\right)^2\right], \tag{4.3}$$

$$\widetilde{K}_{\tilde{\chi}} = \frac{1}{2}\left(\frac{\partial\tilde{\chi}}{\partial\tilde{t}}\right)^2, \qquad \widetilde{G}_{\tilde{\chi}} = \frac{1}{2}\frac{1}{a^2(\tilde{t})}\left[\left(\frac{\partial\tilde{\chi}}{\partial\tilde{x}}\right)^2 + \left(\frac{\partial\tilde{\chi}}{\partial\tilde{y}}\right)^2 + \left(\frac{\partial\tilde{\chi}}{\partial\tilde{z}}\right)^2\right]; \tag{4.4}$$

where we note that the scale factor a is dimensionless. The inflationary potentials and the interaction term eqs. (2.22), (2.23) and (2.24) get re-scaled as,

$$\widetilde{V}(\tilde{\varphi}) = \frac{1}{2}\,\frac{1}{\beta^2\lambda_{\rm E}^2}\,\left(1 - e^{-\lambda_{\rm E}\beta\tilde{\varphi}}\right)^2, \tag{4.5}$$

$$\widetilde{V}(\tilde{\varphi}) = \frac{1}{2}\,\frac{1}{\beta^2\lambda_{\rm T}^2}\,\tanh^2(\lambda_{\rm T}\beta\tilde{\varphi})\,, \tag{4.6}$$

$$\widetilde{\mathcal{I}}(\tilde{\varphi},\tilde{\chi}) = \frac{1}{2}\,q\,\tilde{\varphi}^2\tilde{\chi}^2\,; \qquad q = g^2\,\beta^2\,\frac{m_p^2}{m^2}\,, \tag{4.7}$$

where we used eq. (3.14) to replace V_0 in terms of m and λ in eqs. (4.5) and (4.7). The field eqs. (2.19) and (2.20) thus take the form

$$\frac{\partial^2\tilde{\varphi}}{\partial\tilde{t}^2} + 3\tilde{H}\,\frac{\partial\tilde{\varphi}}{\partial\tilde{t}} - \frac{\widetilde{\boldsymbol{\nabla}}^2}{a^2}\,\tilde{\varphi} + \tilde{V}_{,\tilde{\varphi}} + \tilde{\mathcal{I}}_{,\tilde{\varphi}} = 0\,, \tag{4.8}$$

$$\frac{\partial^2\tilde{\chi}}{\partial\tilde{t}^2} + 3\tilde{H}\,\frac{\partial\tilde{\chi}}{\partial\tilde{t}} - \frac{\widetilde{\boldsymbol{\nabla}}^2}{a^2}\,\tilde{\chi} + \tilde{\mathcal{I}}_{,\tilde{\chi}} = 0\,, \tag{4.9}$$

with

$$\tilde{H}^2 \equiv \left(\frac{{\rm d}\ln a}{{\rm d}\tilde{t}}\right)^2 = \frac{\beta^2}{3}\left(\widetilde{K}_{\tilde{\varphi}} + \widetilde{G}_{\tilde{\varphi}} + \widetilde{V}(\tilde{\varphi}) + \widetilde{K}_{\tilde{\chi}} + \widetilde{G}_{\tilde{\chi}} + \widetilde{\mathcal{I}}(\tilde{\varphi},\ \tilde{\chi})\right). \tag{4.10}$$

We define the re-scaled energy densities and pressures for $\tilde{\varphi}$ and $\tilde{\chi}$ as[3]

$$\tilde{\rho}_{\tilde{\varphi}} = \widetilde{K}_{\tilde{\varphi}} + \widetilde{G}_{\tilde{\varphi}} + \widetilde{V}(\tilde{\varphi}) + \widetilde{\mathcal{I}}(\tilde{\varphi},\tilde{\chi}), \qquad \tilde{p}_{\tilde{\varphi}} = \widetilde{K}_{\tilde{\varphi}} - \frac{1}{3}\widetilde{G}_{\tilde{\varphi}} - \widetilde{V}(\tilde{\varphi}) - \widetilde{\mathcal{I}}(\tilde{\varphi},\tilde{\chi}) \tag{4.11}$$

$$\tilde{\rho}_{\tilde{\chi}} = \widetilde{K}_{\tilde{\chi}} + \widetilde{G}_{\tilde{\chi}}, \qquad \tilde{p}_{\tilde{\chi}} = \widetilde{K}_{\tilde{\chi}} - \frac{1}{3}\widetilde{G}_{\tilde{\chi}} \tag{4.12}$$

[3]We note that due to the way in which $\mathcal{C}$osmo$\mathcal{L}$attice is configured, interaction terms such as $\widetilde{\mathcal{I}}(\tilde{\varphi},\tilde{\chi})$ have to be absorbed within the definition of a potential in the output files, which we do above by including it in the potential of the inflaton, i.e. as $\widetilde{V}(\tilde{\varphi}) + \widetilde{\mathcal{I}}(\tilde{\varphi},\tilde{\chi})$.

JCAP10(2024)082

with their respective equation of state (EoS) parameters

$$\widetilde{w}_{\tilde{\varphi}} = \frac{\widetilde{p}_{\tilde{\varphi}}}{\widetilde{\rho}_{\tilde{\varphi}}}\,, \quad \widetilde{w}_{\tilde{\chi}} = \frac{\widetilde{p}_{\tilde{\chi}}}{\widetilde{\rho}_{\tilde{\chi}}}\,. \tag{4.13}$$

Furthermore, we have defined the dimensionless total energy density and pressure of the system as,

$$\widetilde{\rho} = \widetilde{K}_{\tilde{\varphi}} + \widetilde{K}_{\tilde{\chi}} + \widetilde{G}_{\tilde{\varphi}} + \widetilde{G}_{\tilde{\chi}} + \widetilde{V}(\tilde{\varphi}) + \widetilde{\mathcal{I}}(\tilde{\varphi}, \tilde{\chi}), \tag{4.14}$$

$$\widetilde{p} = \widetilde{K}_{\tilde{\varphi}} + \widetilde{K}_{\tilde{\chi}} - \frac{1}{3}\Big(\widetilde{G}_{\tilde{\varphi}} + \widetilde{G}_{\tilde{\chi}}\Big) - \widetilde{V}(\tilde{\varphi}) - \widetilde{\mathcal{I}}(\tilde{\varphi}, \tilde{\chi}) \tag{4.15}$$

with the associated total EoS parameter

$$\widetilde{w} = \frac{\widetilde{p}}{\widetilde{\rho}}. \tag{4.16}$$

Finally we have defined the *fractional energy density* of different components $F = \{K, G, V, \mathcal{I}\}$, with $f = \{\varphi,\ \chi\}$ as,

$$\varepsilon_F^{\tilde{f}} = \frac{\widetilde{F}(\tilde{f})}{\widetilde{\rho}}\,. \tag{4.17}$$

We note that the dynamics of inflaton decay in the simulations depend primarily on the values of the two key parameters, $\{\lambda,\, g^2\}$, denoting the strengths of the self and external interactions respectively. In tables 1 and 2, we present the values of the self-coupling λ (denoted as $\lambda_{\rm E}$ and $\lambda_{\rm T}$) and the external coupling g^2, along with the corresponding values of V_0 and initial conditions $\{\phi_{\rm in},\, \dot{\phi}_{\rm in}\}$, for the E- and the T-model potentials that are used in our lattice simulations. In our simulations, we consider values of λ that are large enough to ensure that the predicted levels of the tensor-to-scalar ratio satisfy the latest CMB bound, namely $r \leq 0.036$ [16, 18]. The value of V_0 for a given λ has been fixed by the CMB normalisation $\mathcal{P}_\zeta = 2.1 \times 10^{-9}$ [15], the details of which can be found in appendix A. The corresponding inflaton mass m is then determined from V_0 and λ using eq. (3.14).

The primary results of this work were obtained by carrying out simulations with a lattice size of $N = 128^3$ and $\tilde{k}_{\rm IR} = 0.05$,[4] (which is the minimum cut-off for the reciprocal lattice $\tilde{k} = \frac{k}{am}$). The system was evolved using the second-order Velocity-Verlet (VV2) algorithm available in $\mathcal{C}$osmo$\mathcal{L}$attice. In order to ensure inflaton fragmentation and oscillon formation in a shallow potential, approximate analytical bounds on the parameters of the potential were obtained in refs. [33, 38]. For example, in the case of a symmetric potential of the form $V(\varphi) = \frac{1}{2}\, m^2\, \varphi^2 - A^{(4)}\, \varphi^4$, the bound on $\lambda_{\rm T}$ was obtained to be

$$\lambda_{\rm T} \gtrsim 54.77 \sqrt{\frac{0.1}{\gamma_{\rm T}}} \tag{4.18}$$

[4]The infrared cut-off $\tilde{k}_{\rm IR}$ is defined as,

$$\tilde{k}_{\rm IR} = \frac{2\pi}{\widetilde{L}}$$

where $\widetilde{L} = Lm$, with L being the comoving length of the cubic lattice. For $\tilde{k}_{\rm IR} = 0.05$, the lattice has sides of comoving length $L = 40\pi\, m^{-1}$.

JCAP10(2024)082

$\boldsymbol{\lambda_{\rm E}}$	$\boldsymbol{V_0}$ $[m_p^4]$	$\boldsymbol{\phi_{\rm in}}$ $[m_p]$	$\boldsymbol{\dot{\phi}_{\rm in}}$ $[m_p^2]$	$\boldsymbol{m}$ $[m_p]$	$\boldsymbol{g^2}$
$50\sqrt{\frac{2}{3}}$	4.8×10^{-13}	0.038	-5.49×10^{-7}	4.00×10^{-5}	0 1.6×10^{-6} 8.0×10^{-6} 4.0×10^{-5}
$100\sqrt{\frac{2}{3}}$	8.5×10^{-14}	0.020	-2.28×10^{-7}	3.37×10^{-5}	0 1.6×10^{-6} 8.0×10^{-6} 4.0×10^{-5}

Table 1. Values of various parameters used in the simulations with the E-model inflaton potential.

$\boldsymbol{\lambda_{\rm T}}$	$\boldsymbol{V_0}$ $[m_p^4]$	$\boldsymbol{\phi_{\rm in}}$ $[m_p]$	$\boldsymbol{\dot{\phi}_{\rm in}}$ $[m_p^2]$	$\boldsymbol{m}$ $[m_p]$	$\boldsymbol{g^2}$
$50\sqrt{\frac{2}{3}}$	8.5×10^{-13}	0.027	-7.41×10^{-7}	5.32×10^{-5}	0 1.6×10^{-6} 8.0×10^{-6} 4.0×10^{-5}
$100\sqrt{\frac{2}{3}}$	6.5×10^{-14}	0.014	-2.06×10^{-7}	2.94×10^{-5}	0 1.6×10^{-6} 8.0×10^{-6} 4.0×10^{-5}

Table 2. Values of various parameters used for the simulations with the T-model inflaton potential.

where $\gamma_{\rm T} \equiv 2A^{(4)}\phi_{\rm in}^2/m^2 \sim \mathcal{O}(1)$. Similarly, for an asymmetric potential of the form $V(\phi) = \frac{1}{2}m^2\phi^2 - A^{(3)}\phi^3$, the corresponding bound on $\lambda_{\rm E}$ was found to be

$$\lambda_{\rm E} \gtrsim 11.55\left(\frac{0.1}{\gamma_{\rm E}}\right) \tag{4.19}$$

where $\gamma_{\rm E} \equiv 2A^{(3)}\phi_{\rm in}/m^2 \sim \mathcal{O}(1)$. These analytic arguments strongly suggest that the inflaton condensate is expected to fragment with our choice of parameters $\{\lambda,\, g^2\}$ given in tables 1 and 2, corresponding to four representative values of g^2 used in our lattice simulations. However, while indicative, the analytical bounds do not completely guarantee the formation of oscillons, for which we need to take into account the non-linear effects. Hence, in order to investigate the formation of oscillons in our set up, we carry out fully non-linear numerical lattice simulations of the scalar field dynamics. Figure 4 provides an illustrative summary of the key results of our numerical investigations in the form of a $\{\lambda,\, g^2\}$ parameter space plot of the E- and the T-model potentials, highlighting regions of inflaton fragmentation and oscillon formation, distinguishing them from regions where oscillon formation is disrupted due to the presence of large external coupling.

Before proceeding further to discuss the results from our lattice simulations, let us recall that the inflaton oscillations around the minimum of the aforementioned asymptotically flat

JCAP10(2024)082

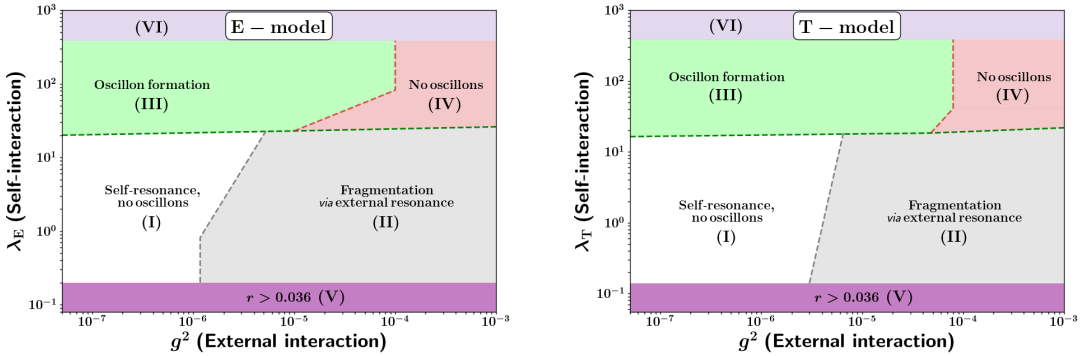

Figure 4. The parameter space, $\{\lambda,\, g^2\}$, of the self and the external coupling constants explored in our lattice simulations for the E-model (*left*) and T-model (*right*) are shown here. Region (I) (shaded in white) corresponds to the parameter space where scalar field fragmentation is negligible, while the inflaton condensate is guaranteed to fragment *via* external resonance, without the formation of oscillons, in region (II) (shaded in grey). The green-shaded region (III) corresponds to the parameter space for which self-interaction is high enough and external coupling is low enough for oscillon formation to take place. However, in region (IV) (red-shaded), oscillon formation is disrupted due to sufficiently high g^2. Region (V) corresponds to $r > 0.036$, which violates the tensor-to-scalar ratio bound. Region (VI) does not host oscillons since the time-averaged EoS of the inflaton is negative and the inflaton mass term is negligible compared to higher-order interactions, as discussed in the text below.

potentials may be tachyonic in nature. In fact, our analysis in appendix C shows that the inflaton oscillations are tachyonic for $\lambda_{\rm T} \geq 0.28$ in the T-model, and for $\lambda_{\rm E} \geq 1.44$ in the E-model, where the effective inflaton mass-squared term $m^2_{\rm eff} \equiv V_{,\phi\phi}$ is negative [100, 101]. This indeed is the case for the chosen values of $\lambda_{\rm E}$, $\lambda_{\rm T}$ in our simulations, as given in tables 1 and 2. For example, figure 19 in appendix C demonstrates that the inflaton condensate explores the tachyonic regime for the first few oscillations before cosmic expansion dampens out the field amplitude (see appendix C for details). Furthermore, for ultra-large values of the self-couplings, namely $\lambda_{\rm E},\, \lambda_{\rm T} \gg \mathcal{O}(10^2)$, the mass terms in the Taylor expansion of the potentials given in eqs. (3.12) and (3.13) become negligible compared to the self-interaction terms. In this case inflaton fragmentation does not lead to oscillon formation, since oscillons are predominantly non-relativistic field configurations [38]. This is shown by the shaded purple region of the parameter space plot in figure 4. We will further explore scalar field fragmentation in the presence of such large self-couplings analytically in our upcoming paper [79].

4.2 Oscillon formation

Our numerical simulations demonstrate that resonant processes during preheating amplify certain $\tilde{k}$ modes within the first few oscillations, $t \sim \mathcal{O}(10^2)\, m^{-1}$. For example, this can be seen for the power spectrum of inflaton fluctuations $\mathcal{P}_{\delta\tilde{\varphi}}(\tilde{k})$ shown in the left panels of figure 5 which is qualitatively different from the initial one (shown in black). This is in excellent agreement with the linear analyses made in section 3 using Floquet theory, where in the left panel of figure 2, we observe that the Fourier modes of inflaton fluctuations with $\tilde{k} \lesssim 0.75$ pass through the broad resonance band in the Floquet chart, which are indicative of the amplifications occurring in $\mathcal{P}_{\delta\tilde{\varphi}}(\tilde{k})$. Larger $\tilde{k}$ modes also experience amplification, albeit at

JCAP10(2024)082

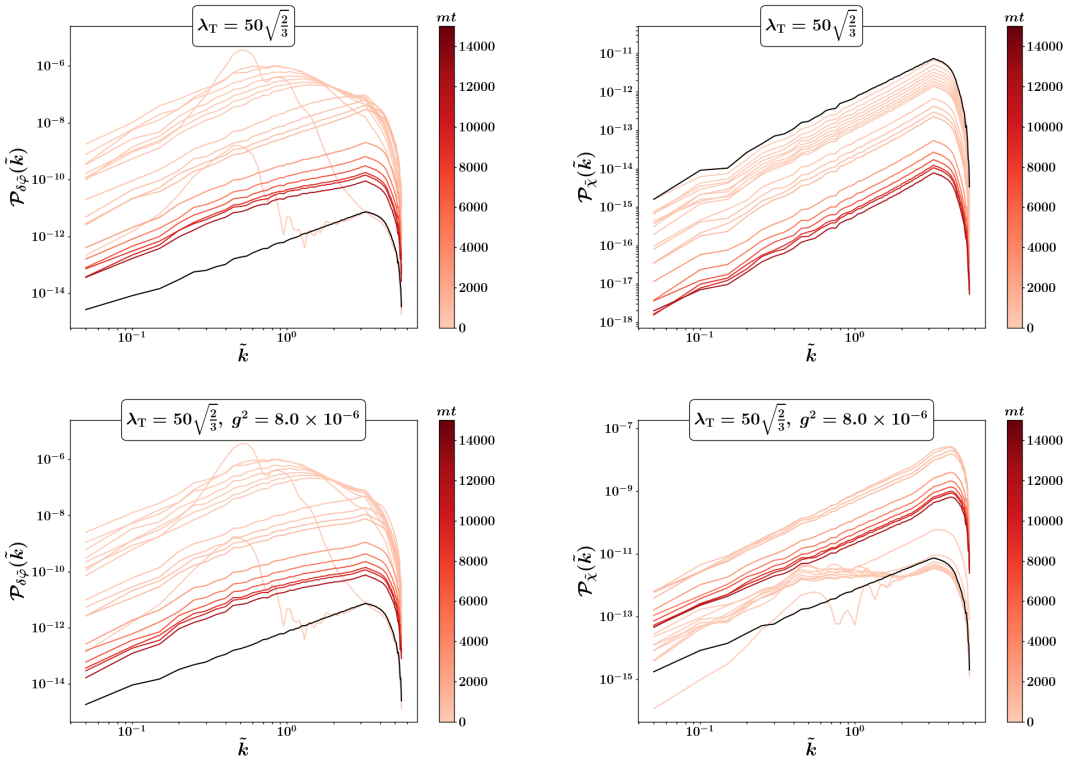

Figure 5. Power spectra of field fluctuations in the T-model, for $\lambda_T = 50\sqrt{2/3}$, in the absence (*top*) and presence (*bottom*) of external coupling obtained from lattice simulations are plotted with the black lines depicting the initial power spectra. The results from lattice simulations are in excellent agreement with the linear analyses in section 3 until $t \sim 100\, m^{-1}$, after which significant backreaction of the field fluctuations onto the homogeneous condensate disrupts the resonant processes. For inflaton fluctuations shown in the left panels, the peaks in the power spectra occurring for $\tilde{k} \lesssim 0.75$ correspond to particle production from the low-momentum modes that traverse the broad-resonance band.

slightly later times, when they pass through the first resonance band in the narrow regime. On the other hand, in the top right panel of figure 5, we see that, in the absence of g^2, the power spectrum of the offspring field $\mathcal{P}_{\delta\tilde{\chi}}(\tilde{k})$ steadily decreases in amplitude with the expansion of the universe. With the interaction term turned on, we observe, in the bottom right panel of figure 5, a gradual amplification in the power spectrum, reflected by the fact that multiple modes cross the various narrow-resonance bands, although the χ-particle production is not as significant as that of the inflaton fluctuations (for the given value of g^2).

We search for the formation of oscillon-like field configurations by analysing the behaviour of the gradient energy density $\widetilde{G}_{\tilde{\varphi}}$ of the inflaton field, as defined in eq. (4.3). At the onset of preheating, we expect the gradient term to provide a subdominant contribution to the total energy density of the system, owing to the fact that significant nonlinearities do not tend to develop towards the end of inflation for smooth asymptotically flat potentials. However, after the first $\sim \mathcal{O}(10^1)$ oscillations, nonlinearities begin to develop on sub-Hubble scales, inducing a rather sharp increase in $\widetilde{G}_{\tilde{\varphi}}$. In figure 6, we showcase the evolution of the volume-averaged fractional energy densities of the fields φ and χ, defined in eq. (4.17), with time (number of

JCAP10(2024)082

e-folds are shown on the upper horizontal axis). For the given values of $\lambda_{\rm E}$, $\lambda_{\rm T}$, we observe that the gradient term $\widetilde{G}_{\varphi}$ of the inflaton field grows considerably within $t \sim 100\, m^{-1}$, contributing an appreciable fraction of the total energy density of the system.

The sharp rise in the gradient term can be understood from figure 7, where the time evolution of the volume-averaged inflaton fluctuation $\sqrt{\delta\widetilde{\varphi}^2}$ is plotted in red. Note that the volume-averaged fluctuation is calculated by first determining the time evolution of the inflaton fluctuations on the $3d$ grid as $\delta\widetilde{\varphi}(\tilde{t}, \widetilde{\boldsymbol{x}}) = \widetilde{\varphi}(\tilde{t}, \widetilde{\boldsymbol{x}}) - \widetilde{\phi}(\tilde{t})$, and then using the definition

$$\langle \delta\widetilde{\varphi}(\tilde{t}, \widetilde{\boldsymbol{x}})^2 \rangle_{\rm V} = \frac{1}{\rm vol} \int_{\rm vol} {\rm d}^3\widetilde{x} \left[\widetilde{\varphi}(\tilde{t}, \widetilde{\boldsymbol{x}}) - \widetilde{\phi}(\tilde{t}) \right]^2 . \tag{4.20}$$

The top panel of figure 7 shows that within $t \lesssim 100\, m^{-1}$ after the end of inflation, a significant amount of inflaton inhomogeneities develop in the E-model, directly translating to the precipitous increase in the gradient term observed in the top left panel of figure 6. We also observe, in the bottom panel of figure 7, that the amplification of inhomogeneities in the T-model is very similar, although slightly quicker, where maximum resonant growth is achieved around $t \sim 50\, m^{-1}$. The enhanced fluctuations then strongly backreact onto the condensate, fragmenting it in the process, with the fragmentation occurring near the peaks of $\delta\widetilde{\varphi}$ and $\widetilde{G}_{\tilde{\varphi}}$. This marks the onset of the backreaction phase, where the oscillations of the inflaton condensate become incoherent, as can be seen in figure 7. Upon fragmentation, the strong attractive self-coupling results in the formation of dense and localised (proto-oscillon) lumps. The time evolution of the lumps is illustrated for the case of no external coupling $g^2 = 0$ in figure 8 in the form of $2d$ spatial slices. Similarly, figures 9 and 10 show the evolution of such lumps as $3d$ constant energy isocontours. Oscillons form from the fragmented inflaton lumps very quickly, in fact, within a duration $\Delta t \sim 20\, m^{-1}$ (in between the inflaton fragmentation and oscillon formation) to be specific. Moreover, they are long-lived — most oscillons in our simulations exhibit a lifetime $\tau_{\rm osc} \sim \mathcal{O}(10^3)\, m^{-1}$ in the absence of any external coupling, while a few continuing to persist even beyond $t \sim 15000\, m^{-1}$. Additionally, they contribute significantly to the energy budget of the system, as will be discussed in section 4.3.

On the other end, in the presence of strong external couplings $g^2 \gtrsim 4 \times 10^{-4}$, we initially observe the formation of inflaton nonlinearities. However, as can be seen in figure 11, these initial nonlinearities are transients, and they quickly dissipate into χ-particles due to the increased coupling strength. Consequently, the system is composed of a bath of fragmented inflaton inhomogeneities and χ-particles. Nevertheless, for intermediate values of the external coupling, i.e. in the range $10^{-6} \lesssim g^2 \lesssim 10^{-4}$, we still observe the formation of nonlinearities within a duration of $\Delta t \sim 20\, m^{-1}$ which clump together to form robust oscillons. Although, such intermediate couplings appear to reduce the longevity and energy fraction of oscillons, which will be discussed in section 4.3. We further note that the values of g^2 quoted above are valid for $\lambda_{\rm E}$, $\lambda_{\rm T} \simeq \mathcal{O}(10^2) \times \sqrt{2/3}$. For lower values of $\lambda_{\rm E}$, $\lambda_{\rm T}$ in the parameter space, the corresponding values g^2 for which oscillon formation is disrupted will be further lowered accordingly.

4.3 The lifetime and decay of oscillons

Oscillons are quasi-stable nonlinear configurations that can be exceptionally long-lived in the absence of an external coupling, (i.e. $g^2 = 0$). There have been numerous studies, both

JCAP10(2024)082

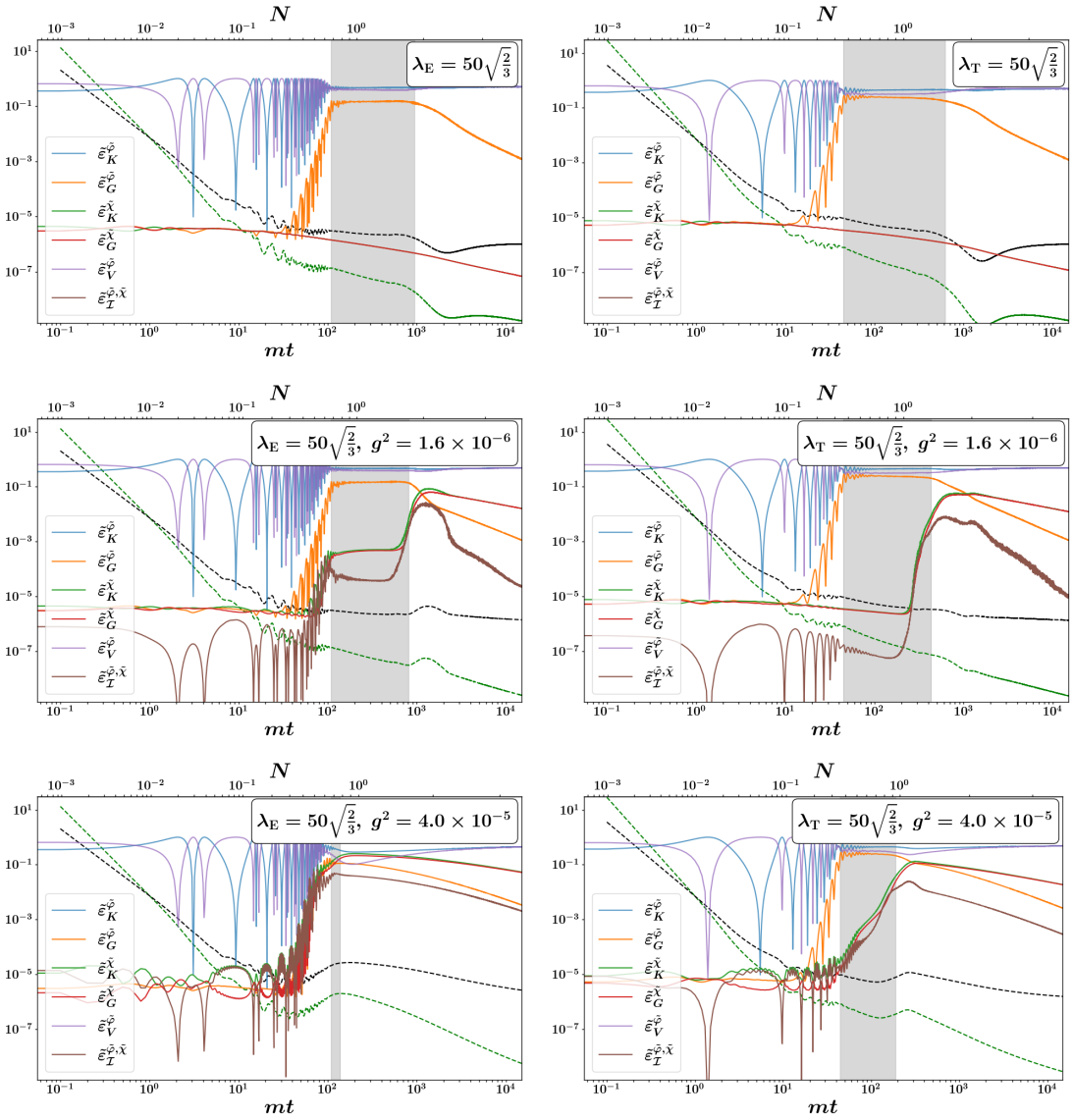

Figure 6. Evolution of the volume-averaged fractional energy density components for $g^2 = 0$ (*top row*), $g^2 = 1.6\times10^{-6}$ (*middle row*) and, $g^2 = 4.0\times10^{-5}$ (*bottom row*) for the E-model (*left column*) and T-model (*right column*) potentials with $\lambda_{\rm E}$, $\lambda_{\rm T} = 50\sqrt{2/3}$ are shown. The shaded regions represent the duration during which $\widetilde{G}_{\tilde{\varphi}} \propto \widetilde{K}_{\tilde{\varphi}}\,(\simeq \widetilde{V}_{\tilde{\varphi}})$. We observe that the gradient energy density of the inflaton $\widetilde{G}_{\varphi}$ grows considerably during preheating due to parametric resonance, which results in the formation of long-lived oscillons in the absence of external coupling. However, although non-linear inflaton lumps (proto-oscillons) do form initially, the presence of a strong enough external coupling, such as $g^2 \gtrsim 4 \times 10^{-5}$, quickly disrupts the formation of robust oscillons, as the newly formed dense fragmented transients of the inflaton quickly dissipate into the χ-particles. From the dashed black and green lines, acting as proxies for the evolution of test matter and radiation fields respectively, we observe that the gradient energy density of the inflaton $\widetilde{G}_{\tilde{\varphi}}$ falls roughly as non-relativistic matter after the formation of oscillons, and as radiation at asymptotically late times.

JCAP10(2024)082

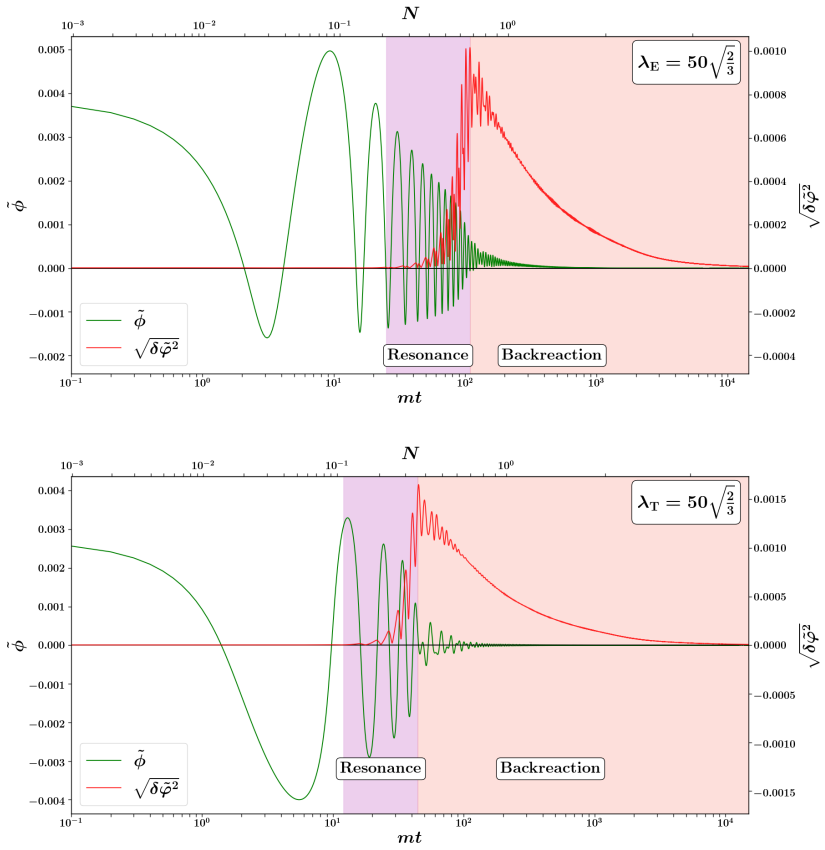

Figure 7. Evolution of the volume-averaged inflaton configurations are plotted for the case $g^2 = 0$ of the E-model (*top panel*) and T-model (*bottom panel*) with $\lambda_{\rm E}$, $\lambda_{\rm T} = 50\sqrt{2/3}$, with the upper horizontal axis being the number of e-folds N elapsed since the end of inflation. Successful self-resonance results in the amplification of $\delta\tilde{\varphi}$, shown here as a solid red line. As a result, the homogeneous inflaton condensate (shown in solid green) fragments within $t \lesssim 100\, m^{-1}$, forming lumps in the process, leading to the formation of oscillons. We note that most oscillons form at the onset of the backreaction phase (the transition from resonance to backreaction phases) near the peak of $\delta\tilde{\varphi}$.

analytical and numerical, on the lifetime and decay of oscillons, some of which can be found in refs. [37, 41, 102–104]. It was confirmed in ref. [37] that the lifetime of an individual oscillon can be extremely long ($10^8\, m^{-1}$), although not *infinite*, based on their analysis with symmetric potentials $V(\varphi) = V(-\varphi)$ using a single-frequency oscillon profile. Furthermore, a class of axion-inspired symmetric potentials was constructed in ref. [104] using a newly developed *physical quasibreather* technique that can sustain the so-called *ultra long-lived oscillons* with lifetimes up to $t \gtrsim 10^{11}\, m^{-1}$ for some specific range of the parameter space of the potentials. The aforementioned analyses were carried out (semi-) analytically to determine the lifetime of a single oscillon.

In this work, since we numerically deal with a population of oscillons, we determine the oscillon lifetime using the time evolution of the gradient and the kinetic (as well as the potential) energy densities of the inflaton field. More specifically, given that oscillons are non-relativistic objects, the lifetime ($\tau_{\rm osc}$) of a population of oscillons can be estimated by

JCAP10(2024)082

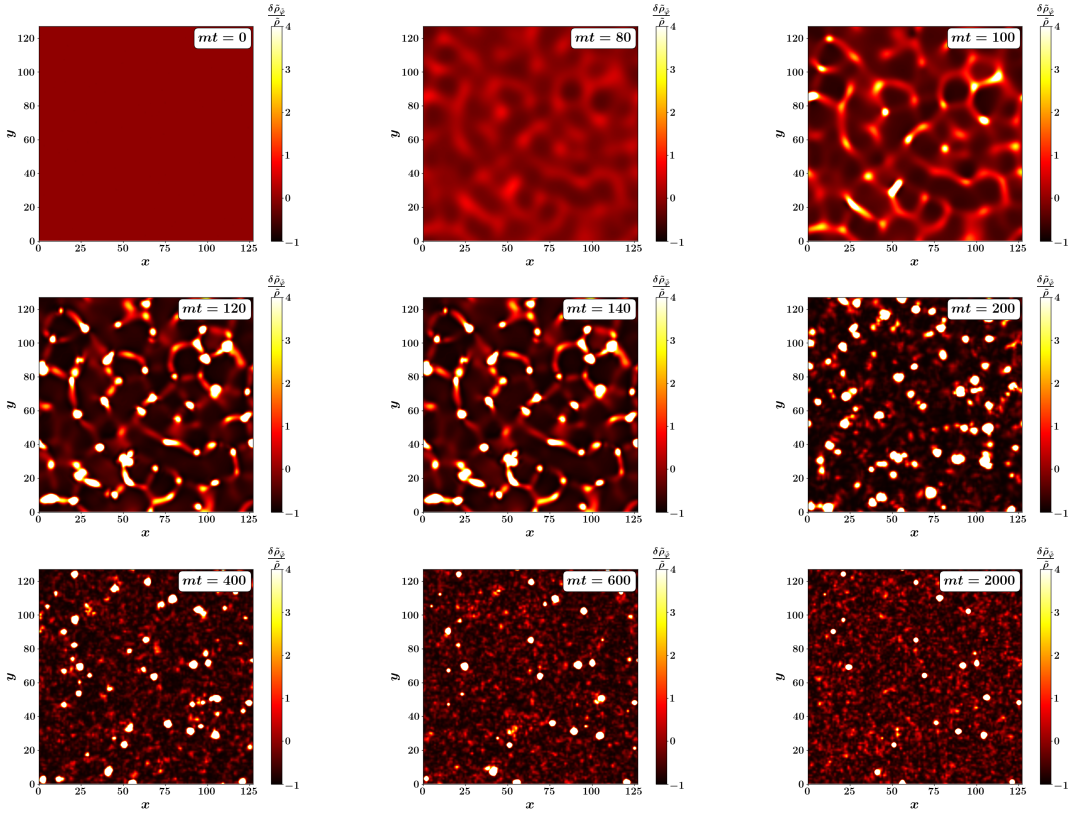

Figure 8. A sequence depicting the formation of oscillons from fragmented inflaton condensate after self-resonance in the E-model, with self-coupling $\lambda_{\rm E} = 50\sqrt{2/3}$ and external coupling $g^2 = 0$. As can be observed, there is significant inflaton fragmentation within the first $t \sim 100\, m^{-1}$, followed by the appearance of oscillon-like localised non-linear structures by $t \sim 120\, m^{-1}$. Hence, oscillons form rather quickly after the inflaton fragmentation, i.e. within a short duration $\Delta t \sim 20\, m^{-1}$. Also notice that most of the oscillons are long-lived, persisting beyond $t \gtrsim 10^3\, m^{-1}$.

comparing the duration for which $\widetilde{G}_{\tilde{\varphi}} \propto \widetilde{K}_{\tilde{\varphi}}\, (\simeq \widetilde{V}_{\tilde{\varphi}}) \propto a^{-3}$. The oscillon lifetime in this work can be categorized based on the type of potential used — symmetric or asymmetric. Using results from the lattice simulations, in particular observing how the gradient energies $\widetilde{G}_{\tilde{\varphi}}$ evolve compared to the energy densities of matter and radiation test fields in an expanding universe, we find that lifetime of oscillons formed in the E-model is relatively longer than their T-model counterparts in the absence of an external coupling. This can be attributed to a stronger self-interaction due to the presence of the cubic term in the Taylor expansion of the E-model potential in eq. (3.12), which is absent in the T-model potential. We intend to carry out a thorough analytical study of the difference between the oscillon lifetimes for the E- and the T-model potentials in an upcoming paper [79].

We find that the presence of a non-vanishing external coupling, $g^2 \neq 0$, can greatly reduce the lifetime of oscillons, as shown in figures 12 and 13. In particular, an increase in the value of g^2 leads to a decrease in oscillon lifetime for a fixed value of the self-coupling $\lambda_{\rm E}$, $\lambda_{\rm T}$. However, the exact functional form of this dependence is difficult to determine directly from the simulations, and this will be the primary goal of our upcoming paper [79].

JCAP10(2024)082

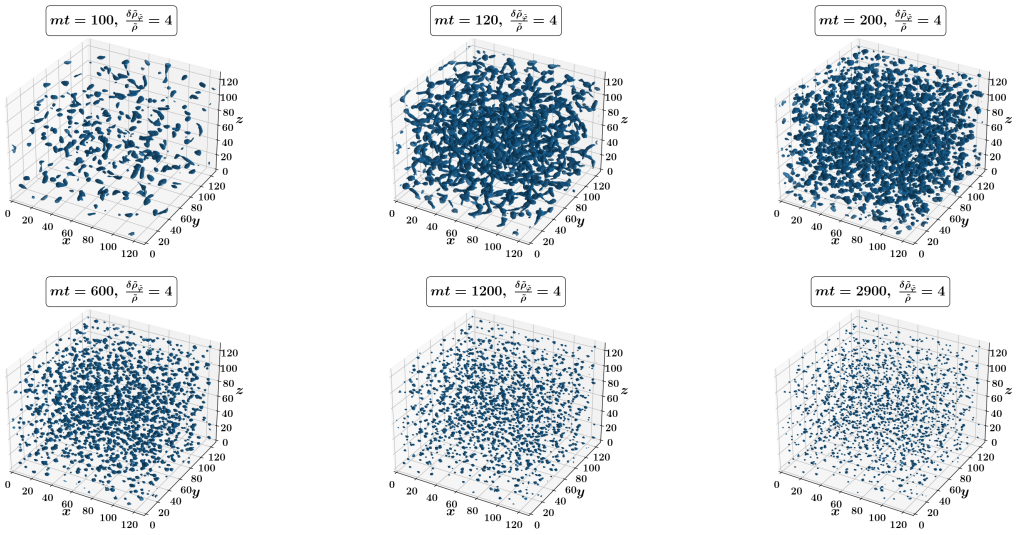

Figure 9. Evolution of the constant density ($3d$) isocontours showing the formation (and relatively slower decay) of oscillons in the absence of an external coupling ($g^2 = 0$) in the E-model ($\lambda_{\rm E} = 50\sqrt{2/3}$) are shown. Note that the sides of the boxes are in the comoving scale. So, oscillons with fixed physical sizes correspond to structures with decreasing comoving size in the figure.

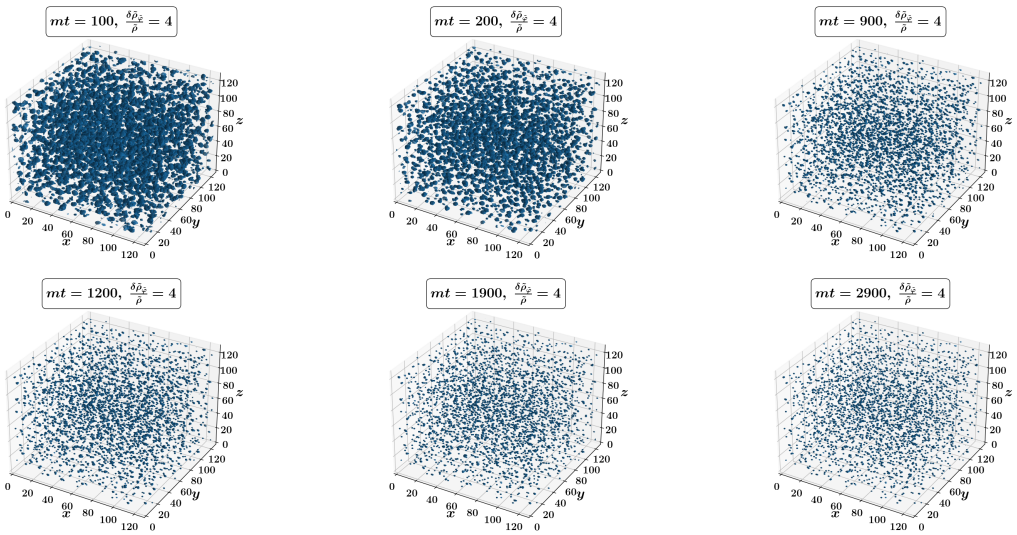

Figure 10. Constant density ($3d$) isocontours showing the formation (and relatively slower decay) of oscillons for $g^2 = 0$ in the T-model with $\lambda_{\rm T} = 50\sqrt{2/3}$.

While very small values of g^2 do not have much impact on their lifetime, for intermediate values of g^2, say $g^2 \in (10^{-6}, 10^{-4})$ the reduction in their lifetimes is quite considerable, as can be seen in table 3. In particular we find that the oscillon lifetime decreases following an approximate *inverse power-law* dependence on g^2, as shown in figure 14. We also find that the (negative) power-law index is higher for E-model oscillons, with $\tau^{\rm E}_{\rm osc} \propto \left(g^2\right)^{-1.1}$, compared to T-model oscillons with $\tau^{\rm T}_{\rm osc} \propto \left(g^2\right)^{-0.3}$.

JCAP10(2024)082

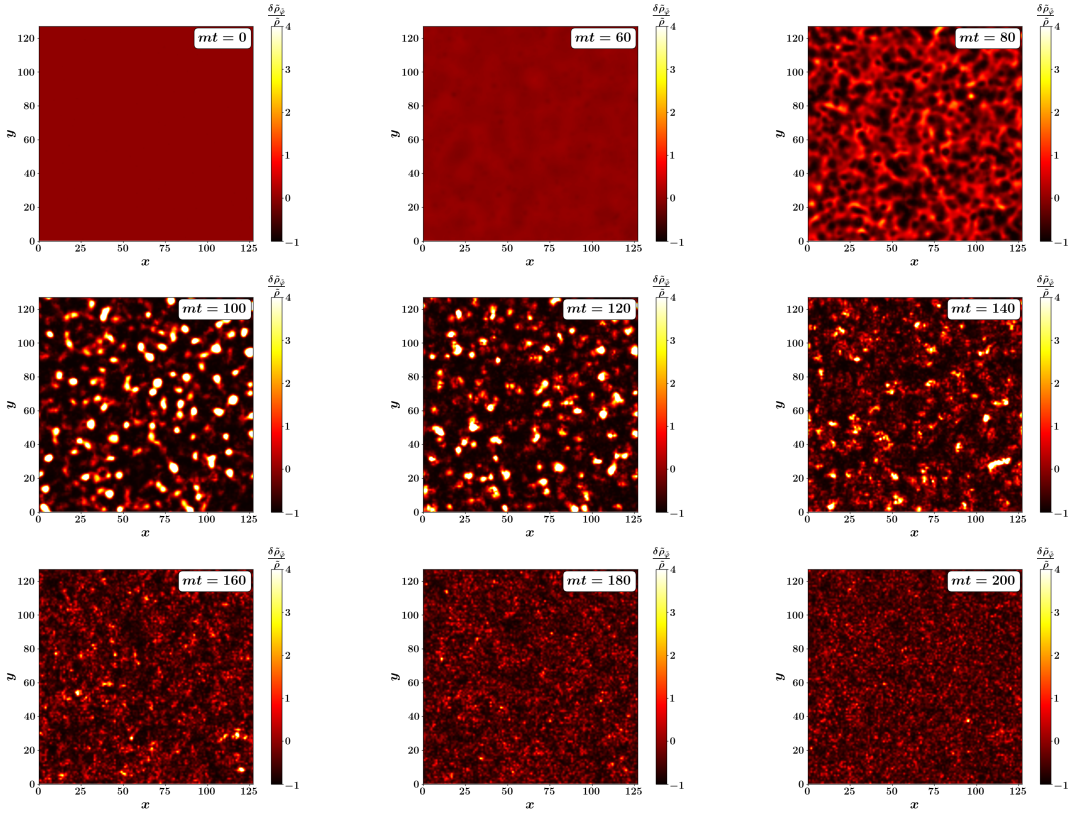

Figure 11. Evolution of the inhomogeneities of the fragmented inflaton condensate after self-resonance in the E-model, with self-coupling $\lambda_{\rm E} = 50\sqrt{2/3}$, and a relatively *large* external coupling $g^2 = 4.0 \times 10^{-5}$ is shown. Note how it now prevents the formation of robust long-lived oscillons, even after a successful period of self-resonance producing large inhomogeneities (proto-oscillons) around $t \sim 100\, m^{-1}$. As a result, any transient dense configuration that forms, quickly dissipates into χ particles, leaving behind a fragmented inflaton field which dominates the energy density of the system.

The reason why the external coupling affects the oscillon lifetime can be understood in terms of decay channels. In the absence of an interaction term ($g^2 = 0$), oscillons are only expected to decay via the emission of scalar radiation which takes place at an exceptionally slow rate due to the stabilising non-linear structure of the oscillons [37, 103, 104]. However, with $g^2 \neq 0$, there is an additional channel [41] through which oscillons can decay, namely oscillons decaying into χ-particles, via $\varphi\,\varphi \to \chi\,\chi$ processes, along with scalar radiation. In particular, figures 9–13 show the progression of oscillon decay for different external couplings by plotting the evolution of the $3d$ constant overdensity isocontours defined as

$$\frac{\delta\widetilde{\rho}_{\tilde{\varphi}}}{\widetilde{\rho}_{\tilde{\varphi}}}(\tilde{t},\widetilde{\boldsymbol{x}}) = \frac{\widetilde{\rho}_{\tilde{\varphi}}(\tilde{t},\widetilde{\boldsymbol{x}}) - \langle\widetilde{\rho}_{\tilde{\varphi}}\rangle_{\rm V}(\tilde{t})}{\langle\widetilde{\rho}_{\tilde{\varphi}}\rangle_{\rm V}(\tilde{t})}\,, \tag{4.21}$$

where the $\langle\ldots\rangle_{\rm V}$ refers to volume-averaging. The axes in these plots are measured in comoving length dimensions. Although the choice of the value of the overdensity isocontours is rather arbitrary, we follow the standard choice in the literature, namely $\delta\rho/\rho \sim \mathcal{O}(1)$. In figures 9 and 10, we see the formation and evolution of these inhomogeneities for the E and T-models with $g^2 = 0$ that persist over a long time-scale. Since resonance and backreaction occur

JCAP10(2024)082

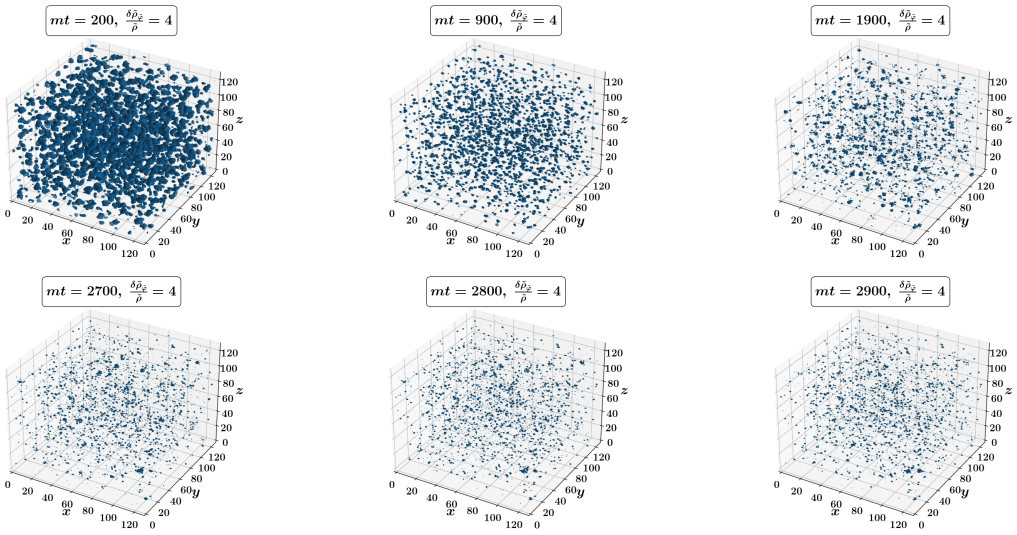

Figure 12. Evolution of the constant density ($3d$) isocontours for sufficiently high external coupling (here $g^2 = 1.6 \times 10^{-6}$ for the E-model $\lambda_{\rm E} = 50\sqrt{2/3}$) shows that oscillons decay to the coupled offspring field χ at a rate greater than that in the absence of the coupling. The rapid decay of oscillons into χ particles is transient and the system is eventually dominated by the slowly decaying inflaton fragments (including oscillons), see the middle row of the left panel of figure 6.

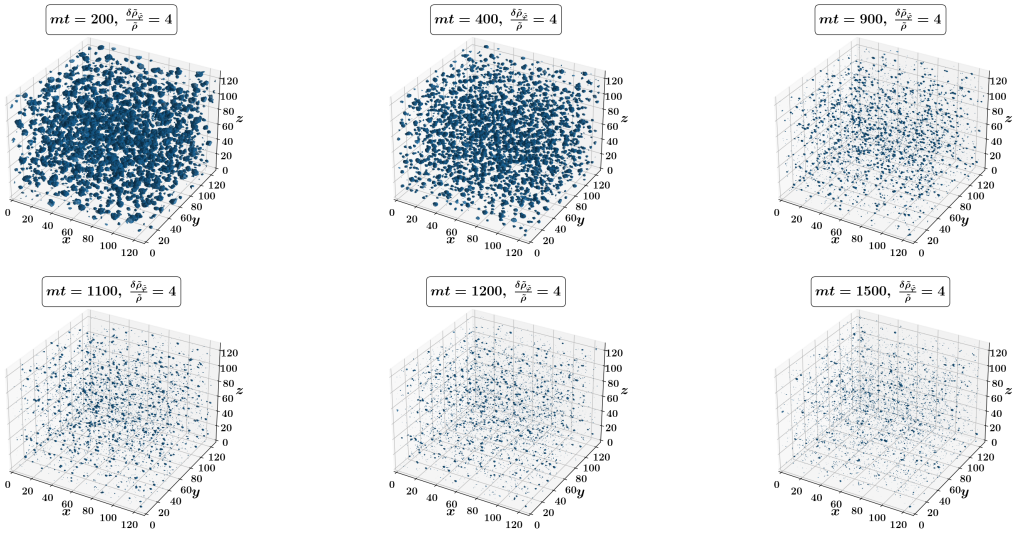

Figure 13. Same as figure 12, but in the presence of a slightly higher external coupling $g^2 = 8.0 \times 10^{-6}$ for the T-model $\lambda_{\rm T} = 100\sqrt{2/3}$.

slightly earlier in the T-model, early signs of inflaton fragmentation can be observed in figure 10. Furthermore, signs of oscillon longevity in the absence of external coupling can be noticed more clearly in the top panel of figure 6.

By comparing the time evolution of $\widetilde{G}_{\tilde{\varphi}}$ with those of the test matter and radiation fields, we see that the gradient energy scales as $\sim a^{-3}$ for time-scales of $\mathcal{O}(10^3)\, m^{-1}$. The production of χ-particles from oscillons when $g^2 \neq 0$ can be explicitly seen to occur at late

JCAP10(2024)082

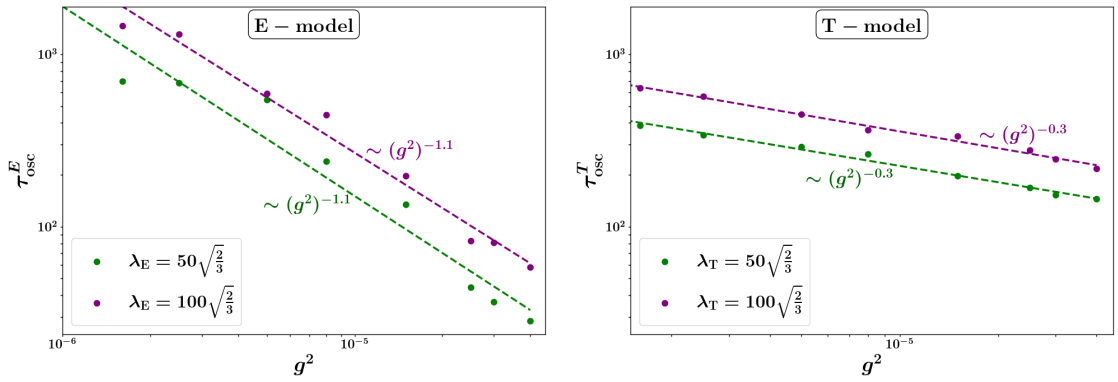

Figure 14. The dependence of the lifetime of (a population of) oscillons, determined here as the duration during which $\widetilde{G}_{\tilde{\varphi}} \propto \widetilde{K}_{\tilde{\varphi}} \, (\simeq \widetilde{V}_{\tilde{\varphi}}) \propto a^{-3}$, as a function of g^2. We note that the oscillon lifetime decreases following an approximate *inverse power-law* dependence on $g^2 \in \left(10^{-6}, 10^{-4}\right)$, which is indicated by the dashed lines (obtained as the best fit curves in the logarithm scale). Furthermore, the (negative) power-law index in the E-model is higher than that in the T-model.

times in figure 15 when the broad band external resonance of the inflaton condensate is absent, (i.e., long after the condensate fragments into oscillons). The effects of nonvanishing g^2 are also shown in figures 12 and 13, where the nonlinear oscillons are observed to dissipate away on much shorter time-scales than in the case of $g^2 = 0$. This is also evident from the evolution of $\widetilde{G}_{\tilde{\varphi}}$ in figure 6. Oscillon decay is also illustrated in the plot for the $2d$ slices of inflaton fluctuations in figure 11. The aforementioned observations illustrate the strong dependence of the strength of the external coupling which is summarised in table 3 and figure 14, as discussed above.

The energy density fraction of oscillons, $f_{\rm osc}$, is defined to be the ratio of the total energy contained within nonlinear configurations, above a suitably chosen threshold, over the total energy. Mathematically, this is given by

$$f_{\rm osc} \equiv \frac{\widetilde{E}_{\rm osc}}{\widetilde{E}_{\rm tot}} = \frac{\int_{\delta\tilde{\rho}>\tilde{\rho}_{\rm th}} {\rm d}^3\widetilde{x} \; \widetilde{\rho}(\tilde{t}, \widetilde{\boldsymbol{x}})}{\int_{\rm vol} {\rm d}^3\widetilde{x} \; \widetilde{\rho}(\tilde{t}, \widetilde{\boldsymbol{x}})} \tag{4.22}$$

We perform the integral in eq. (4.22) for a threshold $\widetilde{\rho}_{\rm th}$ four times the volume-averaged energy density. We emphasize that there is no widely accepted choice for $\widetilde{\rho}_{\rm th}$, although it is usually taken to be in between $\widetilde{\rho}_{\rm th} \in [2\,\widetilde{\rho},\, 5\,\widetilde{\rho}]$. For example, refs. [30, 39] used $\widetilde{\rho}_{\rm th} = 2\,\widetilde{\rho}$ in their calculation of the oscillon fraction. The choice of this threshold will, of course, affect the corresponding value of $f_{\rm osc}$. In this work, we fix the threshold to be $\widetilde{\rho}_{\rm th} = 4\,\widetilde{\rho}$.

The oscillon energy fraction is plotted in figure 16 which demonstrates that $f_{\rm osc}$ rapidly increases at early times during the period of strong self-resonance, reaching a maximum around the onset of the backreaction phase marked by $t \sim 100\, m^{-1}$. This is expected since the gradient term $\widetilde{G}_{\tilde{\varphi}}$ also experiences its maximal amplification during this period, as can be seen from figure 6. In the absence of g^2, the purple curves show that $f_{\rm osc}$ can become as high as 60% at the onset of the backreaction phase, which later asymptotes towards a slightly smaller value of $\approx 50\%$. Furthermore, for $g^2 = 0$ we find that the oscillon energy

JCAP10(2024)082

$\lambda_{\rm E}, \lambda_{\rm T}$	g^2	Oscillon Lifetime (m^{-1})	
		$\tau^{\rm E}_{\rm osc}$	$\tau^{\rm T}_{\rm osc}$
$50\sqrt{\frac{2}{3}}$	0	833.8	479.3
	1.6×10^{-6}	697.3	386.5
	2.5×10^{-6}	681.1	340.0
	5.0×10^{-6}	544.7	290.2
	8.0×10^{-6}	238.7	264.2
	1.5×10^{-5}	134.4	196.5
	2.5×10^{-5}	44.5	167.9
	3.0×10^{-5}	36.5	152.4
	4.0×10^{-5}	28.3	145.2
$100\sqrt{\frac{2}{3}}$	0	1797.7	962.7
	1.6×10^{-6}	1464.0	637.6
	2.5×10^{-6}	1308.2	569.0
	5.0×10^{-6}	591.9	450.4
	8.0×10^{-6}	444.0	363.0
	1.5×10^{-5}	196.9	335.0
	2.5×10^{-5}	84.5	277.5
	3.0×10^{-5}	81.1	246.5
	4.0×10^{-5}	58.1	216.5

Table 3. Lifetime of oscillons in the presence of $\frac{1}{2}g^2\varphi^2\chi^2$ interaction.

fraction $f_{\rm osc}$ saturates to comparatively lower values for larger self-coupling $\lambda_{\rm E}$, $\lambda_{\rm T}$. Such an observation was first made for the E-model potential in ref. [39].[5]

Noticeably, we observe that for the E-model, an external coupling strength of $g^2 = 4.0 \times 10^{-5}$ is sufficient enough to prevent abundant growth of inflaton inhomogeneities in the first place. This can be seen from the red curves in the left column of figure 16, where for $g^2 = 4.0 \times 10^{-5}$, the peak values of $f_{\rm osc} \lesssim 0.3$ ($\lesssim 30\%$ of the total energy budget), even at the onset of backreaction at $t \sim 100\, m^{-1}$. This is in stark contrast to the other three curves, corresponding to smaller values of g^2 in the top panels of figure 16.

Nevertheless, of greater importance is the asymptotic value of $f_{\rm osc}$ at late times. In the presence of $g^2 \in (10^{-6}, 10^{-4})$, even though $f_{\rm osc}$ initially reaches peak values similar to that of $g^2 = 0$, the presence of the additional decay channel results in reduced asymptotic values of the oscillon fraction, i.e. $f_{\rm osc} \lesssim 0.3$ at late times. In particular, for $g^2 \gtrsim \mathcal{O}(10^{-5})$, the final fraction $f_{\rm osc}$ can be less than 10% of the total energy budget. The reduction in the value of $f_{\rm osc}$ in between $t \sim$ (few) $100\, m^{-1}$ and $t \sim$ (few) $1000\, m^{-1}$ corresponds to the rapid decay of oscillons into χ-particles, which is consistent with (the grey shaded region) in figure 15. The remaining oscillons (inflaton lumps) then continue to decay into both χ-particles and scalar radiation at a much slower rate, hence the asymptotic values of $f_{\rm osc}$ exhibit a slow-decay trend towards $t \sim 10^4\, m^{-1}$, as can be seen in figure 16.

[5] In ref. [39], the strength of the self-interaction is controlled by α, where $\lambda_{\rm E} = \sqrt{\frac{2}{3\alpha}}$.

JCAP10(2024)082

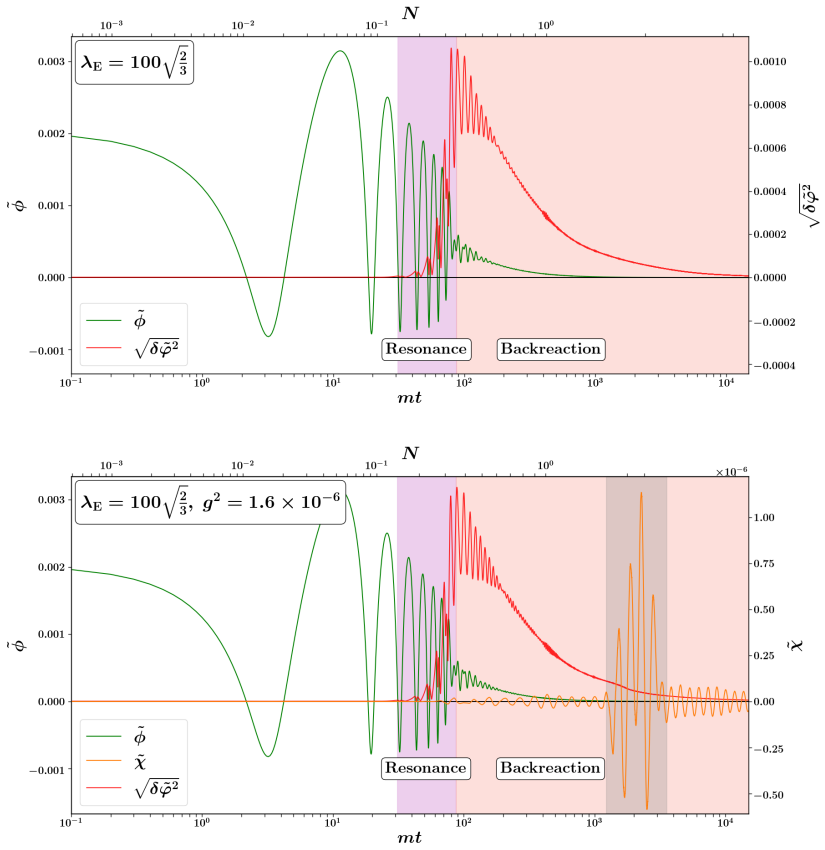

Figure 15. Evolution of the volume-averaged inflaton configurations for the E-model potential with $\lambda_{\rm E} = 100\sqrt{2/3}$ with external couplings $g^2 = 0$ (*top*) and $g^2 = 1.6 \times 10^{-6}$ (*bottom*) are shown. We notice that strong self-resonance leads to the formation of large inflaton inhomogeneities (oscillons) by $t \sim 100\, m^{-1}$, which eventually decay into the χ fluctuations starting from $t \sim 10^3\, m^{-1}$, initially rapidly (shown in light grey shade), and later in a slow and steady rate. Therefore, the presence of such an external coupling significantly impacts the lifetime and fractional energy of oscillons.

Note that for large enough external coupling, corresponding to $g^2 \gtrsim 4 \times 10^{-5}$, the red curves show that $f_{\rm osc}$ exhibits a slowly increasing (instead of decreasing) trend. This is due to the contribution from the interaction term $\widetilde{\mathcal{I}}(\tilde{\varphi}, \tilde{\chi})$ in eq. (4.11), which is usually negligible as compared to that of the gradient term $\widetilde{G}_{\tilde{\varphi}}$ for $g^2 < \mathcal{O}(10^{-5})$. However, the interaction term becomes significant (if not dominant) for $g^2 > \mathcal{O}(10^{-5})$, as can be seen from the brown curves in the bottom panel of figure 6. Hence, for large values of g^2, the late time asymptote of $f_{\rm osc}$ is not completely dictated by oscillons.

5 Discussion and conclusions

Oscillons are nonrelativistic quasi-solitonic field configurations, where attractive non-linear self-interactions enable them to exhibit lifetimes that are far longer than any natural time scale appearing in the Lagrangian. Since they are often investigated during the initial stages of reheating following the end of inflation with a shallow potential, a quantitative understanding of the dynamics of their formation and evolution in a realistic post-inflationary scenario is

JCAP10(2024)082

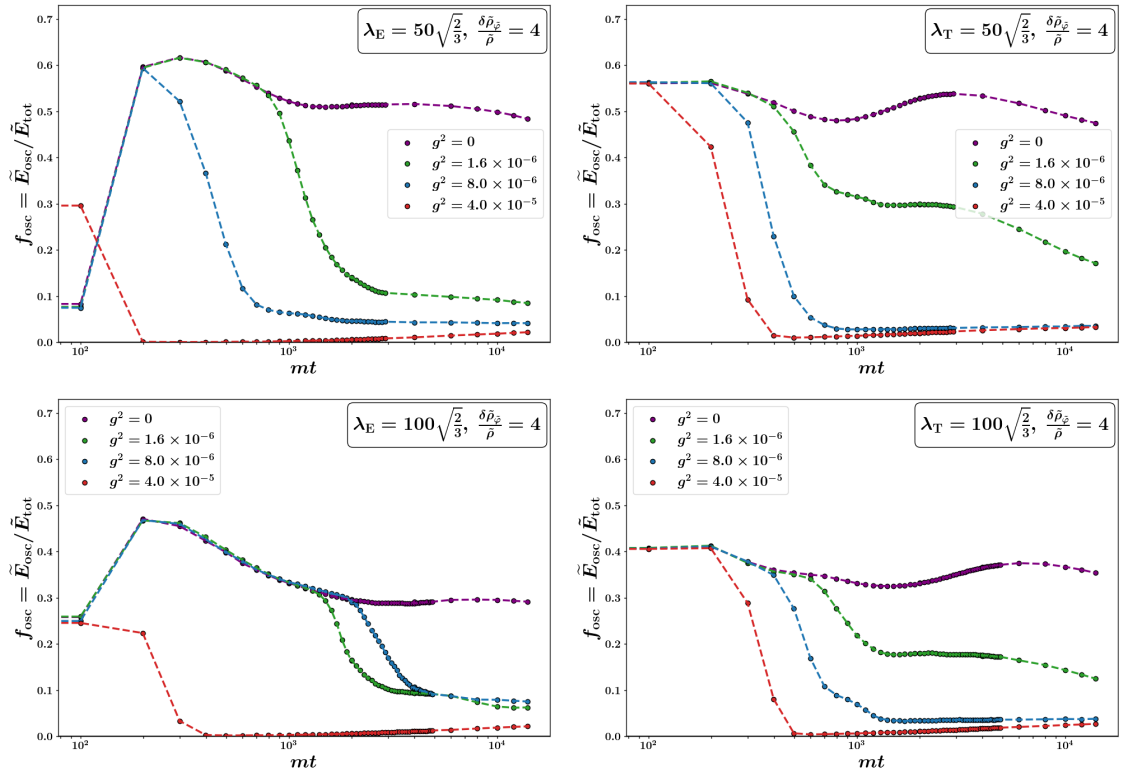

Figure 16. The fractional energy contained in oscillons $f_{\rm osc}$ for different external couplings associated with the E-model (*left*) and T-model (*right*) is shown for $\lambda = 50\sqrt{2/3}$ (*top*) and $\lambda = 100\sqrt{2/3}$ (*bottom*). For $g^2 = 0$ (purple curves), after reaching its peak value following the onset of backreaction, the fraction $f_{\rm osc}$ for each plot then decreases to a near-constant value at late times. The presence of the external coupling leads to a rapid decay where the late-time (near-constant) asymptote of $f_{\rm osc}$ tends to be much lower than that in the case of $g^2 = 0$.

crucial. The majority of papers in the literature have carried out the study of the formation, evolution, and decay of oscillons in the post-inflationary epoch for an isolated self-interacting scalar field, in the absence of any external interactions[6] (with the exception of minimal gravitational coupling). However, if such objects were to form in the early universe *via* fragmentation of the inflaton condensate, they can potentially store a significant fraction of the inflaton energy density that was supposed to decay into other particles in order to reheat the universe. This raises a number of important questions, such as, *(i)* do oscillons form in the presence of (non-negligible) external couplings ?, *(ii)* if yes, then how does the strength of the external coupling affect the lifetime of oscillons ?, and *(iii)* how does the efficiency of preheating get modified in such a decaying inflaton-oscillon scenario ? It is therefore of great interest, both from the phenomenological standpoint of understanding the role of oscillons in reheating, and in establishing in general how couplings to other fields affect their lifetime, to carry out a dedicated quantitative study in this direction.

[6]See ref. [41] for a study of the quantum decay of an oscillon *via* an external coupling. Also, see ref. [72] for a study of oscillon formation and decay based on (2+1)-dimensional lattice simulations of preheating in a hilltop inflaton potential with a quadratic-quartic type external coupling.

JCAP10(2024)082

In this paper, we have taken the first steps towards such an analysis by studying oscillon formation and decay during preheating in two classes of asymptotically flat inflaton potentials where the inflaton (φ) is coupled to a single massless scalar (χ) via an interaction $\mathcal{I} = \frac{1}{2}\, g^2\varphi^2\chi^2$. We started out with the (semi-)analytical study of preheating in the linear regime *via* parametric resonance in order to establish the parameter space for which an exponential growth of inflaton fluctuations is observed at the earliest stages of preheating which is a necessary condition for oscillon formation. In order to firmly establish the formation of oscillons, we then moved on to solve the fully non-linear coupled field equations numerically, using the $\mathcal{C}$osmo$\mathcal{L}$attice framework, which enabled us to carry out a comprehensive study of the formation and decay of oscillons, along with estimating their lifetime and fractional energy density.

Our results are, perhaps, best illustrated by figure 4 where we show the interplay between the self-coupling (λ) and the external coupling (g^2) in determining the dynamics of preheating. In particular, we have identified and demarcated five distinct regions of interest in the parameter space $\{\lambda,\, g^2\}$ of the couplings. For both E- and T-models, consistency with inflationary predictions for primordial GWs rule out a region of the parameter space corresponding to low values of the self-interaction coupling (λ). This includes cases where $\lambda < \mathcal{O}(10^{-1})$ for both potentials. On the other hand, extremely large self-couplings of the order $\lambda \gtrsim 4 \times \mathcal{O}(10^2)$ correspond to situations where the mass term of the inflaton becomes negligible compared to the higher-order self-interaction terms. In such a situation, preheating leads to the formation of fragmented transients which do not clump together as oscillons, since oscillons (by nature) are non-relativistic configurations with vanishing EoS parameter. In fact, if λ is large enough, then the oscillating inflaton field spends most of its time in the plateau region of the potential, leading to an EoS $\langle w_\phi \rangle < -1/3$, in which case the universe continues to accelerate (on the average) for a few post-inflationary oscillations [105]. Such a scenario is termed as *oscillating inflation* [106, 107].

More importantly, we identify the regions in $\{\lambda,\, g^2\}$ parameter space which give rise to inflaton fragmentation, with and without the formation of oscillons, since fragmentation does not always guarantee the formation of oscillons. In particular, we find that oscillon formation occurs in both E- and T-models above a certain threshold value of $\lambda \sim \mathcal{O}(10)$, which agrees well with the previous studies in refs. [34, 38, 39] for $g^2 = 0$. In the presence of external coupling, we observe the formation of robust oscillons for $g^2 \lesssim 10^{-4}$. Of equal significance is the fact that the lifetime of these oscillons is strongly dependent on the magnitude of g^2, as summarised in table 3. Oscillon lifetimes for both E- and T-model potentials can then be suitably fitted in the interval of interest $g^2 \in (10^{-6}, 10^{-4})$ and are shown in figure 14, where it can be seen that $\ln g^2$ and $\ln \tau_{\rm osc}$ are approximately linear. Stated differently, g^2 and $\tau_{\rm osc}$ satisfy an approximate power-law relation with a negative index, i.e. an *inverse power-law* relation. We found that for both values of self couplings $\lambda_{\rm E} = \lambda_{\rm T} = 50\sqrt{2/3}$ and $100\sqrt{2/3}$, the oscillon lifetimes fall as

$$\tau^{\rm E}_{\rm osc} \propto \left(g^2\right)^{-1.1}; \qquad \tau^{\rm T}_{\rm osc} \propto \left(g^2\right)^{-0.3}. \tag{5.1}$$

The aforementioned observations raise the obvious question of why the lifetimes are different between the two models with the E-model producing longer living oscillons while

JCAP10(2024)082

also displaying more efficient decay with the increase in g^2. In the absence of the external coupling, we find that $\tau_{\rm osc}^{\rm E} \approx 2\tau_{\rm osc}^{\rm T}$ in units of m^{-1}, which is a noticeable difference. Similarly, one may wonder whether or not an approximate functional form exists relating $\tau_{\rm osc}$ and g^2 (and whether or not it stays a power-law of the form $\tau_{\rm osc} \sim (g^2)^{-\gamma}$) for other inflationary models. Admittedly, it is difficult to explain these nuances in this work (based on lattice simulations), which rather warrants a dedicated separate study. We wish to address them in our upcoming paper [79], which will be devoted to an analytical study of oscillon decay in the presence of such an external coupling.

Regardless of these subtleties, we have demonstrated that the post-inflationary universe can be populated with these oscillons and that, in the correct circumstances, they can constitute a significant fraction of the energy density, which will be of cosmological importance if they are sufficiently long-lived. Even if they are short-lived, the prospects of studying reheating through oscillon decay appears to be fascinating. Since the primary goal of this work is to study the formation and decay of oscillons, we did not carry out a study of the end stages of reheating marked by $\langle w \rangle \to 1/3$, which necessarily requires the inclusion of additional couplings, and involves numerical codes simulating the Boltzmann equations [108, 109]. (Although, we did carry out a thorough analysis of the evolution of the EoS during preheating via inflaton and oscillon decay, which can be found in appendix D.)

Nevertheless, it remains to be seen how different external couplings (Yukawa and trilinear couplings) and (or) the presence of several massless scalar fields modify the preheating dynamics. Various stages of (p)reheating, along with the associated complex high energy dynamics, are of great phenomenological interest to cosmologists, since they carry crucial prospects for the detection of a stochastic gravitational wave (GW) background. In fact, both oscillon formation and decay are expected to seed second-order GWs because of the large source terms arising from non-vanishing anisotropic stresses. It is well-known that oscillon formation (or even inflaton fragmentation in general [110, 111]) is accompanied by high-frequency (GHz-scale) stochastic GWs [36, 63]. Even though such GWs are beyond the sensitivities of the current and proposed detectors, potentially significant progress in the development of resonant cavity detectors [112–116] is expected in the upcoming decade, which will enable them to achieve enough sensitivity to detect the high-frequency cosmological GWs [117]. Of greater interest is the fact that rapid decay of oscillons carries its own GW signatures that can be well within the sensitivities of current and proposed detectors [118].

Before concluding, it is worth mentioning that, as with most cosmological lattice studies, our analysis has been carried out without incorporating the effects of metric perturbations that are important for the evolution of long wavelength fluctuations at relatively late times. As a result, we do not quantify the influence that gravitational interactions have on the preheating dynamics and the formation of oscillons (and importantly, on oscillon lifetimes [103]). Metric perturbations, if accounted for, usually present themselves in the form of the gauge-invariant Bardeen potential Φ_k in the equation of motion of the inflaton fluctuations, and can induce additional Floquet instability in the system, including in potentials that otherwise would not exhibit resonant growth of fluctuations. For example, the inflaton fluctuations at the bottom of a purely quadratic potential can be written in a way that resembles the Mathieu equation in the presence of metric perturbations, giving rise to the *metric preheating* [119–121] scenario.

JCAP10(2024)082

In fact, working in the framework of numerical relativity[7] affords one greater control of computing the amplification of density contrast, along with the usual metric perturbations, which is ideal in refining the selection criteria for nonlinear compact structures such as the oscillons and oscillatons [123, 124]; even allowing us to study the formation of primordial black holes (PBHs) [54, 57, 125] through the detection of apparent horizon formation [57].

Acknowledgments

MS was supported by the INSPIRE scholarship of the Department of Science and Technology (DST), Govt. of India during his Master's thesis work during which a significant portion of this work was carried out. SSM and EJC are supported by STFC Consolidated Grant [ST/T000732/1]. EJC is also supported by a Leverhulme Research Fellowship [RF- 2021 312]. SSM thanks IUCAA, Pune for their hospitality. We thank Paul Saffin for useful discussions. Numerical simulations were carried out on the Padmanabha HPC cluster at IISER TVM. For the purpose of open access, the authors have applied a CC BY public copyright license to any Author Accepted Manuscript version arising.

Data availability statement. This work is entirely theoretical and has no associated data. The data files for the lattice simulations (with the exception of the $3d$ configuration files) and other codes can be found in the following GitHub repository: https://github.com/RM503/Oscillons.

A Inflationary predictions of the E- and T-model potentials

The parameters derived in tables 1 and 2 are fixed by taking into account inflationary constraints arising from the CMB. In this appendix, we explain how the CMB constraints can be used to set the parameters for the lattice simulations analytically. Derivation of the expressions for various inflationary quantities used below can be found in refs. [6, 99]. The E- and T-model potentials are given by

$$V(\phi)\big|_{\text{E-model}} = V_0\left(1 - e^{-\lambda_{\text{E}}\frac{\phi}{m_p}}\right)^2,$$
$$V(\phi)\big|_{\text{T-model}} = V_0 \tanh^2\left(\lambda_{\text{T}}\frac{\phi}{m_p}\right).$$

The initial field value ϕ_{in} is conventionally chosen to be the value of the inflaton field at which the inflationary phase terminates ϕ_{end}. We can analytically determine this using the first potential slow-roll parameter[8]

$$\epsilon_V = \frac{m_p^2}{2}\left(\frac{V_{,\phi}}{V}\right)^2, \tag{A.1}$$

where the end of inflation corresponds to $\epsilon_V(\phi_{\text{end}}) = 1$. This condition can then be used to solve for ϕ_{end}. Using eq. (A.1) for the E- and T-model potentials, we arrive at the

[7] GRChombo [122] is an example of an open-source numerical relativity code that can be used to study scalar field dynamics in the early universe.

[8] The first potential slow-roll parameter is approximately equal to ϵ_H defined in eq. (2.13) during slow-roll.

JCAP10(2024)082

following expressions

$$\phi_{\rm end} = \begin{cases} \dfrac{m_p}{\lambda_{\rm E}} \ln\left(\sqrt{2}\lambda_{\rm E} + 1\right); & \text{E-model}, \\ \dfrac{m_p}{2\lambda_{\rm T}} \text{arccosech}\left(2\sqrt{2}\lambda_{\rm T}\right); & \text{T-model}. \end{cases} \tag{A.2}$$

The inflaton mass m defined in section 4 can be determined using the CMB normalisation of the curvature power spectrum at the pivot scale, which we denote as $\mathcal{P}_{\zeta\star}$. In the slow-roll regime, this can be calculated using [6, 99]

$$\mathcal{P}_{\zeta\star} \simeq \frac{1}{12\pi^2} \frac{V^3(\phi_\star)}{V_{,\phi}^2(\phi_\star) m_p^6}, \tag{A.3}$$

where the '$\star$' subscripts represent evaluations at the pivot scale $k_\star = 0.05\,\text{Mpc}^{-1}$. In order to determine the field value $\phi_\star$ at the Hubble exit of the pivot scale, we use the relation between the elapsed number of e-folds and the inflaton field excursion (following directly from eq. (2.11))

$$N(\phi_\star) \equiv \Delta N = \frac{1}{m_p^2} \int_{\phi_{\rm end}}^{\phi_\star} \mathrm{d}\phi \, \frac{V}{V_{,\phi}}, \tag{A.4}$$

the number of e-folds can be related to $\phi_\star$. After the integral is carried out, the resulting expression can be inverted and $\phi_\star$ can be calculated for the required elapsed e-folds ΔN. For the E-model potential, we obtain

$$\lambda_{\rm E} \frac{\phi_\star}{m_p} = -2\lambda_{\rm E}^2 \Delta N + \lambda_{\rm E} \frac{\phi_{\rm end}}{m_p} - e^{\lambda_{\rm E} \frac{\phi_{\rm end}}{m_p}} - W_{-1}\left[-\exp\left(-2\lambda_{\rm E}^2 \Delta N + \lambda_{\rm E} \frac{\phi_{\rm end}}{m_p} - e^{\lambda_{\rm E} \frac{\phi_{\rm end}}{m_p}} \right) \right], \tag{A.5}$$

where W_{-1} is the '-1 branch' of the Lambert W function [98]. For the T-model potential, we have

$$\lambda_{\rm T} \frac{\phi_\star}{m_p} = \frac{1}{2} \text{arccosh}\left[8\lambda_{\rm T}^2 \Delta N + \cosh\left(2\lambda_{\rm T} \frac{\phi_{\rm end}}{m_p} \right) \right]. \tag{A.6}$$

Eqs. (A.5) and (A.6), along with the CMB normalisation $\mathcal{P}_{\zeta\star} = 2.1 \times 10^{-9}$, can then be used to constrain V_0 for different choices of λ thereby constraining m.

Although the aforementioned analytical approach was presented based on the slow-roll approximations, in practice, given that slow-roll approximations break down towards the end of inflation, we determined the parameters in tables 1 and 2 numerically, in order to be more accurate.

B Relation between number of e-folds and number of oscillations

For homogeneous scalar field oscillations around a quadratic potential, the time-averaged EoS vanishes, i.e. $\langle w_\phi \rangle = 0$, leading to a matter dominated expansion. The same is also true when the scalar field fragments to form oscillons. So in both the cases, we have

$$\langle \rho_\phi \rangle = \rho_i \left(\frac{a_i}{a} \right)^3.$$

JCAP10(2024)082

Substituting this into the Friedmann equation

$$\frac{\dot{a}}{a} = \sqrt{\frac{\rho_i}{3m_p^2}\left(\frac{a_i}{a}\right)^3},$$

and integrating from initial time t_i to some time t, we obtain

$$a(t) = a_i\left[1 + \frac{\sqrt{3}}{2}\left(\frac{\rho_i}{m_p^2}\right)^{1/2}(t - t_i)\right]^{2/3}$$

which leads to

$$t - t_i = \sqrt{\frac{4}{3}}\left(\frac{m_p^2}{\rho_i}\right)^{1/2}\left[\left(\frac{a}{a_i}\right)^{3/2} - 1\right].$$

Since the period of oscillations is given by $T = 2\pi/m$, where m is the mass of the field, the number of oscillations is given by

$$\frac{t - t_i}{T} \equiv n_{\rm osc} = \frac{1}{\sqrt{3\pi^2}}\frac{m\, m_p}{\sqrt{\rho_i}}\left[e^{\frac{3}{2}\Delta N} - 1\right]. \tag{B.1}$$

Noting that close to the minimum of the potential, $\rho_i \simeq \rho_e = 3/2\, V(\phi) = 3/4\, m^2\phi_i^2$, we get the final expression for the number of oscillations to be

$$n_{\rm osc} = \frac{2}{3\pi}\left(\frac{m_p}{\phi_i}\right)\left[e^{\frac{3}{2}\Delta N} - 1\right], \tag{B.2}$$

or equivalently

$$\Delta N = \frac{2}{3}\ln\left[1 + \frac{3\pi}{2}\left(\frac{\phi_i}{m_p}\right)n_{\rm osc}\right]. \tag{B.3}$$

For example, assuming $\phi_i = 2m_p/(3\pi)$, the number of e-folds of expansion after 10^3 oscillations is given by $\Delta N \simeq 4.6$, indicating that oscillons which decay after 1000 oscillations live up to 4.6 e-folds of expansion. Note that eq. (B.3) is not applicable when the EoS deviates substantially from $w = 0$.

C Post-inflationary tachyonic oscillations

The Fourier modes of the inflaton fluctuations $\delta\varphi_k$ satisfy the equation of a damped oscillator with a time-dependent frequency of the form (see eq. (3.7))

$$\ddot{\delta\varphi}_k + 3H\dot{\delta\varphi}_k + \left[\frac{k^2}{a^2} + V_{,\phi\phi}(\phi)\right]\delta\varphi_k = 0\,. \tag{C.1}$$

After the end of inflation, as the inflaton rolls down towards the minimum of the potential, there may be a region in the field space where its effective mass-squared term becomes negative, i.e.,

$$m_{\rm eff}^2(\phi) \equiv V_{,\phi\phi}(\phi) < 0\,. \tag{C.2}$$

JCAP10(2024)082

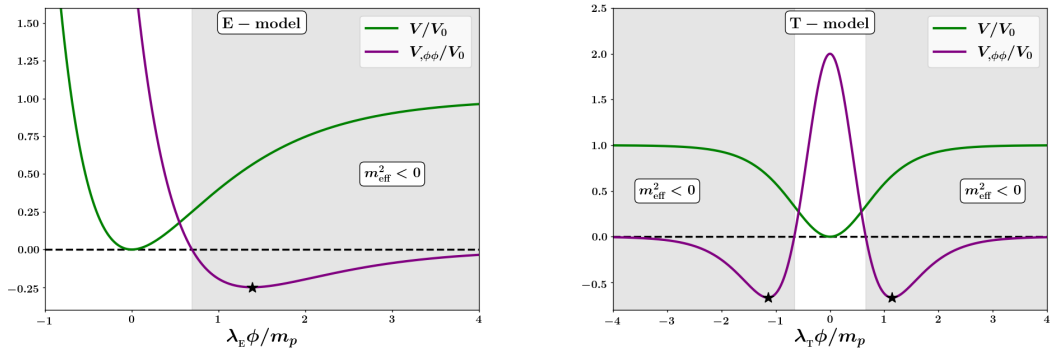

Figure 17. An illustration of tachyonic regions in the E-model (*left*) and T-model (*right*) potentials for which $m^2_{\rm eff} < 0$. The '⋆' marks indicate the points for which the corresponding $m^2_{\rm eff}$ values are at their minima (most-negative).

In such a region, the infrared modes of $\delta\varphi_k$ for which $k^2/a^2 + V_{,\phi\phi} < 0$ grow exponentially, triggering *tachyonic instability* which offers a preheating channel distinct from the standard parametric resonance (where particle production occurs due to non-adiabatic time variation of the effective mass-squared term). During the course of oscillations, the inflaton condensate exhibits repeated field excursions to either sides of the inflection point, marked by $V_{,\phi\phi}(\phi_{\rm inflection}) = 0$, giving rise to *tachyonic oscillations*. The number of tachyonic oscillations depend on $\phi_{\rm in}$ (and hence on λ) as well as on the evolution of the Hubble friction term. Tachyonic instability is a common feature of many hilltop-type models [73] and asymptotically flat potentials [126, 127].

The tachyonic instability region for the E-model potential (2.22) is shown in the left panel of figure 17. The grey shaded region indicates the presence of a negative $m^2_{\rm eff}(\phi)$, with the boundary given by

$$\frac{\lambda_{\rm E}\phi}{m_p} = \ln 2\,. \tag{C.3}$$

Similarly, for the T-model potential (2.23), the grey-shaded regions in the right panel of figure 17 indicate a negative $m^2_{\rm eff}$, with boundaries

$$\frac{\lambda_{\rm T}\phi}{m_p} = \frac{1}{2}\ln\left(2 \pm \sqrt{3}\right). \tag{C.4}$$

The '⋆' marks indicate points in the field space where the corresponding $m^2_{\rm eff}$ values are at their minima (maximally negative).

A simple way to infer the existence of tachyonic oscillations is the following. The inflaton oscillations are tachyonic if it performs field excursions to either sides of the inflection point, defined by

$$\eta_V(\phi_{\rm inflection}) \equiv m_p^2\left(\frac{V_{,\phi\phi}}{V}\right)\Bigg|_{\phi=\phi_{\rm inflection}} = 0\,, \tag{C.5}$$

after the end of inflation. This is possible only if the inflection point satisfies $|\phi_{\rm inflection}| < |\phi_{\rm end}|$. Hence, the existence of tachyonic oscillations in the α-attractor models ultimately depends

JCAP10(2024)082

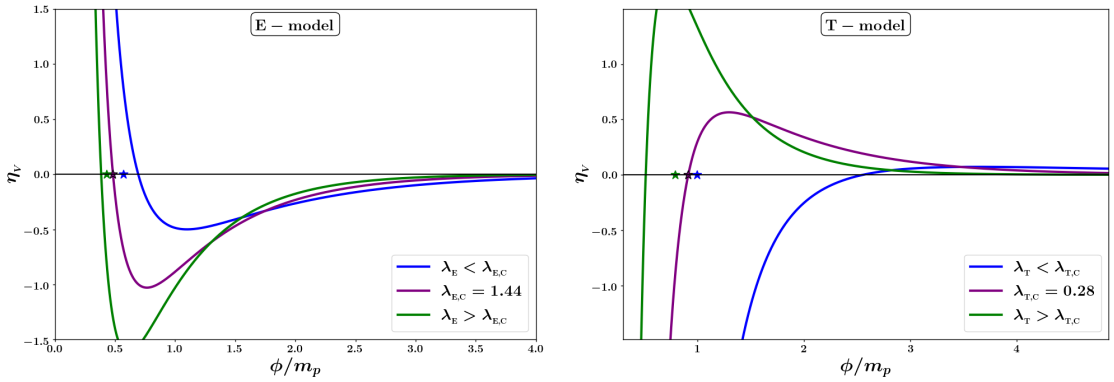

Figure 18. The figures illustrate how the possibility of exhibiting tachyonic oscillations in the E-model (*left*) and T-model (*right*) potentials depends upon the value of λ. Post-inflationary oscillations are tachyonic when the inflaton makes excursions to either side of $\eta_V(\phi_{\rm inflection}) = 0$. The '$\star$' marks correspond to field values ($\phi_{\rm end}$) at the end of inflation, i.e. $\epsilon_H(\phi_{\rm end}) = 1$. The corresponding condition for post-inflationary tachyonic oscillations becomes $\phi_{\rm inflection} < \phi_{\rm end}$, which is achieved for $\lambda > \lambda_{\rm E,C} = 1.44$ (for E-model) or $\lambda > \lambda_{\rm T,C} = 0.28$ (for T-model).

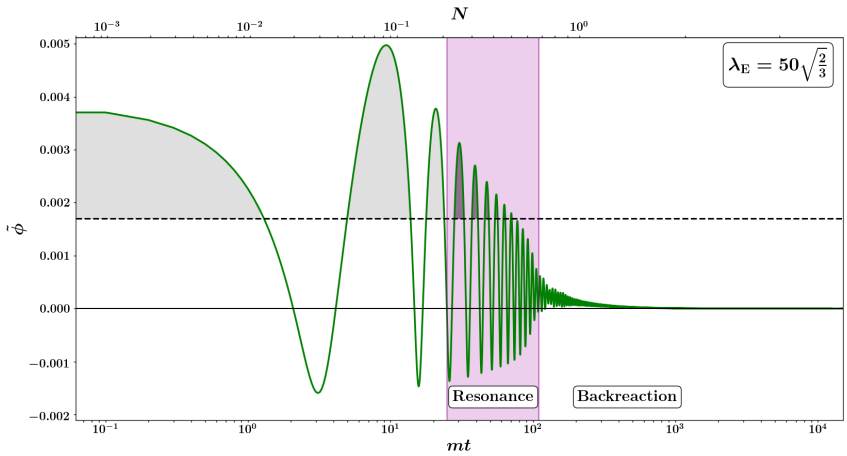

Figure 19. Time evolution of the homogeneous inflation condensate (with the upper horizontal axis being the number of e-folds N elapsed since the end of inflation) is shown here for the E-model with $\lambda_{\rm E} = 50\sqrt{2/3}$. The grey shaded regions above the dashed line correspond to the regimes of tachyonic oscillations, which are absent at late times, since the field amplitude decreases due to Hubble friction (as well as due to self-resonance).

upon the value of λ in eqs. (2.22) and (2.23). Figure 18 demonstrates that for $\lambda_{\rm E,C} > 1.44$ for the E-model, and for $\lambda_{\rm T,C} > 0.28$ for the T-model, the first few post-inflationary oscillations are tachyonic. Tachyonic oscillations for the E-model potential with $\lambda_{\rm E} = 50\sqrt{2/3}$ is shown by the grey shaded regions in figure 19. We note that the oscillations cease to be tachyonic at late times, since the field amplitude decreases due to Hubble friction (as well as due to self-resonance and particle production in general).

JCAP10(2024)082

D The impact of the formation and decay of oscillons on the equation of state

The asymptotic value towards which the equation of state (EoS) of the system eventually settles depends on the nature of the self-interaction potential near the minimum (quadratic or not, up to the leading order) as well as on the presence of inhomogeneities. Much like the way a system of self-gravitating masses virialises, it can be shown that the post-inflationary scalar field dynamics, under the influence of an attractive self-interaction, also eventually virialises,[9] obeying [34, 128]

$$\left\langle \left(\frac{\partial \tilde{f}}{\partial \tilde{t}} \right)^2 \right\rangle_{\mathrm{V,T}} = \left\langle \left(\frac{\widetilde{\boldsymbol{\nabla}} \tilde{f}}{a} \right)^2 \right\rangle_{\mathrm{V,T}} + \left\langle \tilde{f} \, \frac{\partial \widetilde{V}}{\partial \tilde{f}} \right\rangle_{\mathrm{V,T}} \quad ; \quad \tilde{f} = \{ \tilde{\varphi}, \tilde{\chi} \} \, , \tag{D.1}$$

where $\langle \cdots \rangle_{\mathrm{V,T}}$ refers to volume and time-averaging and $\widetilde{V}$ takes into account the interaction term as well (here, it is a shorthand for $\widetilde{V} + \widetilde{\mathcal{I}}$). Since both the E- and T-model potentials behave as $V(\varphi) \propto \varphi^{2n}$ (with $n = 1$) near their minima (up to the leading order), we find that the virialisation condition in eq. (D.1) can be expressed as

$$\begin{aligned} \frac{1}{2} \left\langle \left(\frac{\partial \widetilde{\varphi}}{\partial \tilde{t}} \right)^2 \right\rangle_{\mathrm{V,T}} &= \frac{1}{2} \left\langle \left(\frac{\widetilde{\boldsymbol{\nabla}} \widetilde{\varphi}}{a} \right)^2 \right\rangle_{\mathrm{V,T}} + n \left\langle \widetilde{V}(\widetilde{\varphi}) \right\rangle_{\mathrm{V,T}} + 2 \left\langle \widetilde{\mathcal{I}}(\widetilde{\varphi}, \widetilde{\chi}) \right\rangle_{\mathrm{V,T}} \, , \\ \left\langle \widetilde{K}_{\tilde{\varphi}} \right\rangle_{\mathrm{V,T}} &= \left\langle \widetilde{G}_{\tilde{\varphi}} \right\rangle_{\mathrm{V,T}} + n \left\langle \widetilde{V}(\widetilde{\varphi}) \right\rangle_{\mathrm{V,T}} + 2 \left\langle \widetilde{\mathcal{I}}(\widetilde{\varphi}, \widetilde{\chi}) \right\rangle_{\mathrm{V,T}} \, , \end{aligned} \tag{D.2}$$

and

$$\begin{aligned} \frac{1}{2} \left\langle \left(\frac{\partial \widetilde{\chi}}{\partial \tilde{t}} \right)^2 \right\rangle_{\mathrm{V,T}} &= \frac{1}{2} \left\langle \left(\frac{\widetilde{\boldsymbol{\nabla}} \widetilde{\chi}}{a} \right)^2 \right\rangle_{\mathrm{V,T}} \, , \\ \left\langle \widetilde{K}_{\tilde{\chi}} \right\rangle_{\mathrm{V,T}} &= \left\langle \widetilde{G}_{\tilde{\chi}} \right\rangle_{\mathrm{V,T}} \, . \end{aligned} \tag{D.3}$$

In the limit where the gradient and the interaction energy densities are subdominant, we notice, using the definition in eq. (4.16), that eqs. (D.2) and (D.3) yield the familiar relation for the EoS parameter

$$\langle \widetilde{w} \rangle_{\mathrm{V,T}} = \frac{n-1}{n+1} \, , \tag{D.4}$$

as expected from a homogeneous condensate.

Evolution of the average EoS obtained for different $\{\lambda, g^2\}$ can then be explained by using the virial condition along with examining the relative variations in the different energy components. Since the self-interaction potentials used in this work possess quadratic minima, i.e. they correspond to $n = 1$, the observed late-time asymptote $\langle \widetilde{w} \rangle_{\mathrm{V,T}} \to 0$ (pressureless dust behaviour) in figures 20 and 21 can be inferred from the relative equal proportions of kinetic and potential energies. This is particularly true at late times when all gradient and

[9] In practice, the system virialises only approximately, in the sense that there will always be residual deviations away from the virial theorem for the averaged energy density components. However, the virial theorem can still be used to explain some of the details of the behaviour of the EoS. The energy density components satisfy the virial theorem to a high degree once the system has evolved for a sufficiently long time.

JCAP10(2024)082

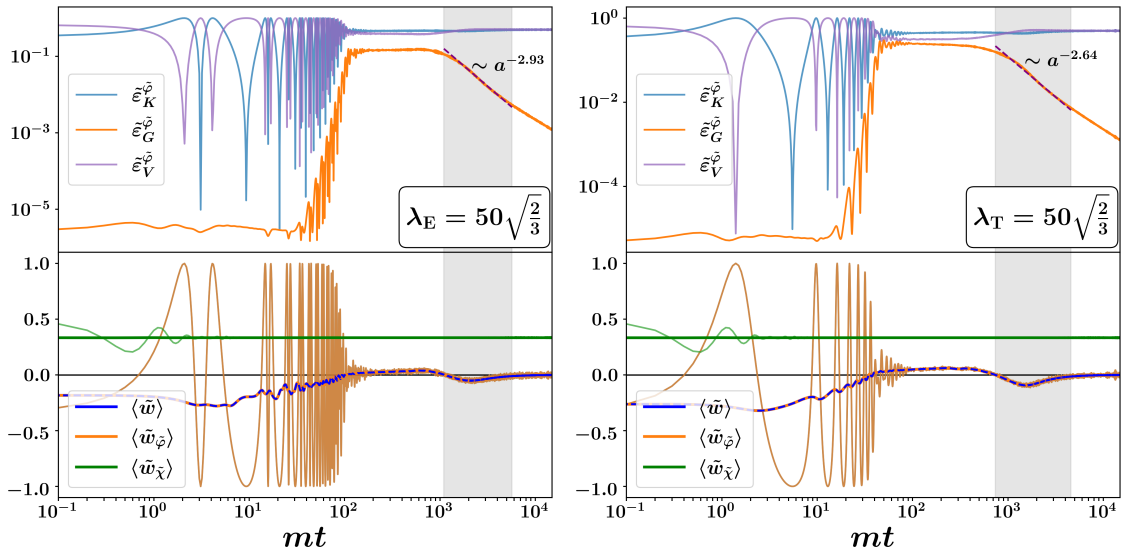

Figure 20. Evolution of the time-averaged equation of state $\langle\widetilde{w}\rangle$ in the absence of an external coupling for the E-model (*left*) and the T-model (*right*) are shown, superposed with the corresponding fractional energy density components $\tilde{\varepsilon}_i$. The positive deviations from $\langle\widetilde{w}\rangle \simeq 0$ are due to the potential term (purple curve) falling below the kinetic term (blue curve) transiently. We also highlight regions where the EoS display negative deviations (in the shaded gray regions) due to the fact that the potential term becomes higher than the kinetic term for a short period (although the sub-dominant gradient term falls faster), prior to achieving virialisation. Nonetheless, as the system evolves, $\langle\widetilde{w}\rangle$ asymptotically approaches zero.

interaction terms become subdominant, while the kinetic and potential terms of $\widetilde{\varphi}$ balance each other out. The EoS of the χ-field does not contribute to the overall EoS, even though $\langle\widetilde{w}_{\widetilde{\chi}}\rangle_{\rm V,T} = 1/3$, since the production of χ-particles is inefficient at late times in the absence of parametric resonance, and the number density of existing χ-particles gets redshifted away. Tiny fluctuations in their number densities may still be observed due to the slow decay of the inhomogeneities in the φ-field into the χ field fluctuations.

Of course, in figure 20 there are deviations away from the $\langle\widetilde{w}\rangle_{\rm V,T} = 0$ behaviour, which is particularly evident during the onset of resonance and backreaction phases and for some period of time afterwards. When $g^2 = 0$, during the resonance and backreaction phases, we know that the gradient energy of the $\widetilde{\varphi}$-field becomes comparable to the kinetic and potential energies. Hence, we find that

$$\langle\widetilde{w}\rangle_{\rm V,T} \approx \frac{1}{3}\left[1 + \frac{\langle\widetilde{V}\rangle_{\rm V,T}}{\langle\widetilde{G}_{\tilde{\varphi}}\rangle_{\rm V,T}}\right]^{-1}, \quad (g^2 = 0)\,. \tag{D.5}$$

Considering that $\langle\widetilde{V}\rangle_{\rm V,T} > \langle\widetilde{G}_{\tilde{\varphi}}\rangle_{\rm V,T}$ during resonance and backreaction, as can be seen in the top panels of figure 6, we can conclude that during these phases

$$0 < \langle\widetilde{w}\rangle_{\rm V,T} < \frac{1}{3}\,. \tag{D.6}$$

To explain the negative deviations in the EoS shortly after backreaction, we refer to the top panel of figure 20 which displays the evolution of the different energy components $\langle\widetilde{E}_i\rangle$,

JCAP10(2024)082

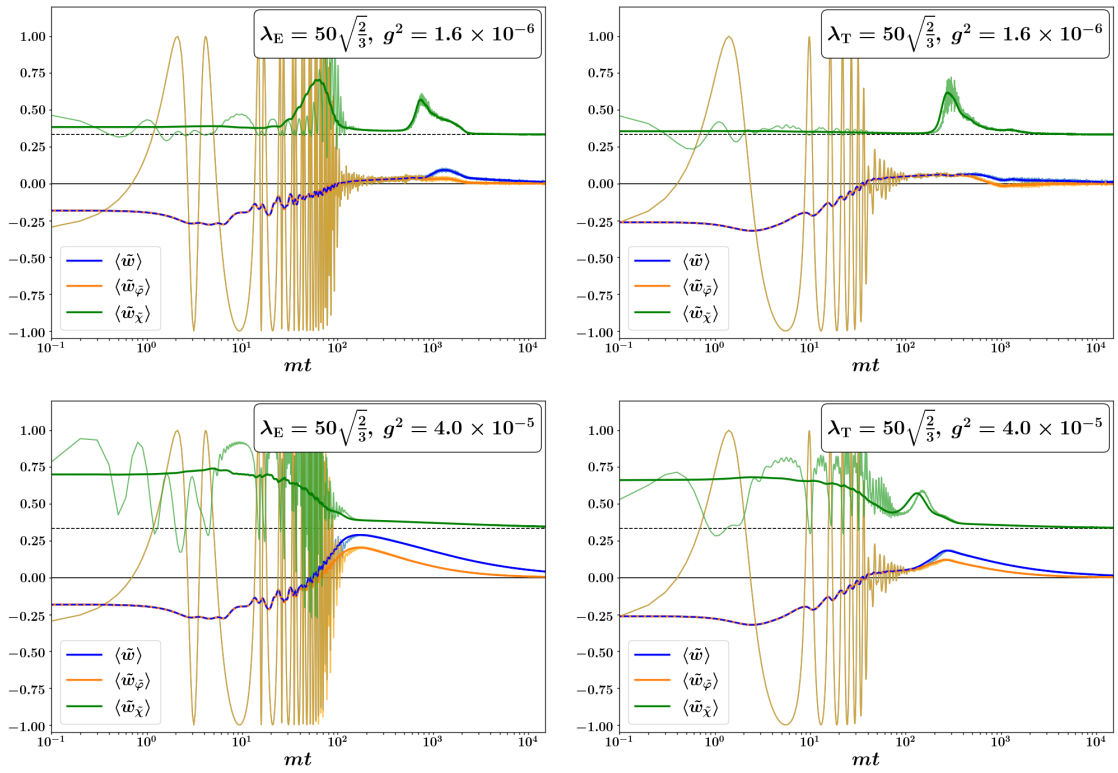

Figure 21. Evolution of the time-averaged equation of state $\langle \widetilde{w} \rangle$ in the presence of an external coupling g^2, for the E-model (*left*) and the T-model (*right*) potentials are shown. The presence of such an external coupling can disrupt the formation (or accelerate the decay) of oscillons. Again, as the system evolves with time, $\langle \widetilde{w} \rangle$ asymptotically approaches zero.

where $i = \{K, G, V\}$, as a fraction of the total energy. It can be observed that $\widetilde{G}_{\tilde{\varphi}} \propto a^{-3}$ for the duration of the backreaction phase (indicative of the inhomogeneities behaving like pressureless matter). Afterwards, however, $\widetilde{G}_{\tilde{\varphi}}$ experiences a rather sharp decline. During this period $\langle \widetilde{V}_{\tilde{\varphi}} \rangle_{\rm V,T} > \langle \widetilde{K}_{\tilde{\varphi}} \rangle_{\rm V,T}$ (only slightly) which we can use to account for the small negative values of the EoS. Approximate scaling relations of the gradient energies are shown in figure 20. Since $\widetilde{\rho}_{\tilde{\varphi}} \propto a^{-3}$, we find that

$$\widetilde{G}_{\tilde{\varphi}} \propto \begin{cases} a^{-5.93}, & \text{(E-model)}\,; \\ a^{-5.64}, & \text{(T-model)}\,. \end{cases} \tag{D.7}$$

For $g^2 \neq 0$, even though the system tends to a matter-dominated phase in the long run, there are more interesting transient behaviour owing to the presence of coupling between the two fields. The $\widetilde{\chi}$-field becomes virialised after the first few oscillations such that $\langle \widetilde{w}_{\tilde{\chi}} \rangle_{\rm V,T} \sim 1/3$. This can also be seen in the middle and bottom panels of figure 6 where $\langle \widetilde{K}_{\tilde{\chi}} \rangle_{\rm V,T}$ and $\langle \widetilde{G}_{\tilde{\chi}} \rangle_{\rm V,T}$ track each other throughout their evolution. There are periods when $\langle \widetilde{w}_{\tilde{\chi}} \rangle_{\rm V,T}$ become stiff, coinciding with periods when $\widetilde{\mathcal{I}}(\widetilde{\varphi}, \widetilde{\chi})$ peaks. However, since the $\widetilde{\chi}$-field only provides a subdominant contribution to the energy of the system, the overall EoS does not become stiff and any period in its evolution, and any positive deviations that arise relax to the EoS of a matter-dominated system.

JCAP10(2024)082

References

[1] A.A. Starobinsky, *A New Type of Isotropic Cosmological Models Without Singularity*, *Phys. Lett. B* **91** (1980) 99 [INSPIRE].

[2] A.H. Guth, *The Inflationary Universe: A possible Solution to the Horizon and Flatness Problems*, *Phys. Rev. D* **23** (1981) 347 [INSPIRE].

[3] A.D. Linde, *A New Inflationary Universe Scenario: A possible Solution of the Horizon, Flatness, Homogeneity, Isotropy and Primordial Monopole Problems*, *Phys. Lett. B* **108** (1982) 389 [INSPIRE].

[4] A. Albrecht and P.J. Steinhardt, *Cosmology for Grand Unified Theories with Radiatively Induced Symmetry Breaking*, *Phys. Rev. Lett.* **48** (1982) 1220 [INSPIRE].

[5] A.D. Linde, *Chaotic Inflation*, *Phys. Lett. B* **129** (1983) 177 [INSPIRE].

[6] D. Baumann, *Inflation*, in the proceedings of the *Theoretical Advanced Study Institute in Elementary Particle Physics: Physics of the Large and the Small*, Boulder, U.S.A., 01–26 June 2009 [DOI:10.1142/9789814327183_0010] [arXiv:0907.5424] [INSPIRE].

[7] V.F. Mukhanov and G.V. Chibisov, *Quantum Fluctuations and a Nonsingular Universe*, *JETP Lett.* **33** (1981) 532 [INSPIRE].

[8] S.W. Hawking, *The Development of Irregularities in a Single Bubble Inflationary Universe*, *Phys. Lett. B* **115** (1982) 295 [INSPIRE].

[9] A.A. Starobinsky, *Dynamics of Phase Transition in the New Inflationary Universe Scenario and Generation of Perturbations*, *Phys. Lett. B* **117** (1982) 175 [INSPIRE].

[10] A.H. Guth and S.Y. Pi, *Fluctuations in the New Inflationary Universe*, *Phys. Rev. Lett.* **49** (1982) 1110 [INSPIRE].

[11] A.A. Starobinsky, *Spectrum of relict gravitational radiation and the early state of the universe*, *JETP Lett.* **30** (1979) 682 [INSPIRE].

[12] V. Sahni, *The Energy Density of Relic Gravity Waves From Inflation*, *Phys. Rev. D* **42** (1990) 453 [INSPIRE].

[13] D. Baumann, *Cosmology*, Cambridge University Press (2022) [DOI:10.1017/9781108937092] [INSPIRE].

[14] Planck collaboration, *Planck 2018 results. VI. Cosmological parameters*, *Astron. Astrophys.* **641** (2020) A6 [*Erratum ibid.* **652** (2021) C4] [arXiv:1807.06209] [INSPIRE].

[15] Planck collaboration, *Planck 2018 results. X. Constraints on inflation*, *Astron. Astrophys.* **641** (2020) A10 [arXiv:1807.06211] [INSPIRE].

[16] BICEP and Keck collaborations, *Improved Constraints on Primordial Gravitational Waves using Planck, WMAP, and BICEP/Keck Observations through the 2018 Observing Season*, *Phys. Rev. Lett.* **127** (2021) 151301 [arXiv:2110.00483] [INSPIRE].

[17] J. Martin, C. Ringeval and V. Vennin, *Encyclopædia Inflationaris*, *Phys. Dark Univ.* **5-6** (2014) 75 [arXiv:1303.3787] [INSPIRE].

[18] S.S. Mishra and V. Sahni, *Canonical and Non-canonical Inflation in the light of the recent BICEP/Keck results*, arXiv:2202.03467 [INSPIRE].

[19] R. Kallosh and A. Linde, *Cosmological Attractors and Asymptotic Freedom of the Inflaton Field*, *JCAP* **06** (2016) 047 [arXiv:1604.00444] [INSPIRE].

JCAP10(2024)082

[20] A. Albrecht, P.J. Steinhardt, M.S. Turner and F. Wilczek, *Reheating an Inflationary Universe*, *Phys. Rev. Lett.* **48** (1982) 1437 [INSPIRE].

[21] E.W. Kolb, *The Early Universe*, CRC Press (1990) [DOI:10.1201/9780429492860] [INSPIRE].

[22] M.S. Turner, *Coherent Scalar Field Oscillations in an Expanding Universe*, *Phys. Rev. D* **28** (1983) 1243 [INSPIRE].

[23] L. Kofman, A.D. Linde and A.A. Starobinsky, *Reheating after inflation*, *Phys. Rev. Lett.* **73** (1994) 3195 [hep-th/9405187] [INSPIRE].

[24] Y. Shtanov, J.H. Traschen and R.H. Brandenberger, *Universe reheating after inflation*, *Phys. Rev. D* **51** (1995) 5438 [hep-ph/9407247] [INSPIRE].

[25] L.A. Kofman, *The origin of matter in the universe: Reheating after inflation*, astro-ph/9605155 [INSPIRE].

[26] L. Kofman, A.D. Linde and A.A. Starobinsky, *Towards the theory of reheating after inflation*, *Phys. Rev. D* **56** (1997) 3258 [hep-ph/9704452] [INSPIRE].

[27] P.B. Greene, L. Kofman, A.D. Linde and A.A. Starobinsky, *Structure of resonance in preheating after inflation*, *Phys. Rev. D* **56** (1997) 6175 [hep-ph/9705347] [INSPIRE].

[28] M.A. Amin, M.P. Hertzberg, D.I. Kaiser and J. Karouby, *Nonperturbative Dynamics Of Reheating After Inflation: A Review*, *Int. J. Mod. Phys. D* **24** (2014) 1530003 [arXiv:1410.3808] [INSPIRE].

[29] K.D. Lozanov, *Lectures on Reheating after Inflation*, arXiv:1907.04402 [INSPIRE].

[30] M.A. Amin et al., *Oscillons After Inflation*, *Phys. Rev. Lett.* **108** (2012) 241302 [arXiv:1106.3335] [INSPIRE].

[31] S.-Y. Zhou et al., *Gravitational Waves from Oscillon Preheating*, *JHEP* **10** (2013) 026 [arXiv:1304.6094] [INSPIRE].

[32] K.D. Lozanov and M.A. Amin, *End of inflation, oscillons, and matter-antimatter asymmetry*, *Phys. Rev. D* **90** (2014) 083528 [arXiv:1408.1811] [INSPIRE].

[33] J. Kim and J. McDonald, *Inflaton Condensate Fragmentation: Analytical Conditions and Application to α-Attractor Models*, *Phys. Rev. D* **95** (2017) 123537 [arXiv:1702.08777] [INSPIRE].

[34] K.D. Lozanov and M.A. Amin, *Self-resonance after inflation: oscillons, transients and radiation domination*, *Phys. Rev. D* **97** (2018) 023533 [arXiv:1710.06851] [INSPIRE].

[35] M.A. Amin et al., *Gravitational waves from asymmetric oscillon dynamics?*, *Phys. Rev. D* **98** (2018) 024040 [arXiv:1803.08047] [INSPIRE].

[36] K.D. Lozanov and M.A. Amin, *Gravitational perturbations from oscillons and transients after inflation*, *Phys. Rev. D* **99** (2019) 123504 [arXiv:1902.06736] [INSPIRE].

[37] H.-Y. Zhang et al., *Classical Decay Rates of Oscillons*, *JCAP* **07** (2020) 055 [arXiv:2004.01202] [INSPIRE].

[38] J. Kim and J. McDonald, *General analytical conditions for inflaton fragmentation: Quick and easy tests for its occurrence*, *Phys. Rev. D* **105** (2022) 063508 [arXiv:2111.12474] [INSPIRE].

[39] R. Mahbub and S.S. Mishra, *Oscillon formation from preheating in asymmetric inflationary potentials*, *Phys. Rev. D* **108** (2023) 063524 [arXiv:2303.07503] [INSPIRE].

[40] G. Fodor, P. Forgacs, Z. Horvath and M. Mezei, *Computation of the radiation amplitude of oscillons*, *Phys. Rev. D* **79** (2009) 065002 [arXiv:0812.1919] [INSPIRE].

JCAP10(2024)082

[41] M.P. Hertzberg, *Quantum Radiation of Oscillons*, *Phys. Rev. D* **82** (2010) 045022 [arXiv:1003.3459] [INSPIRE].

[42] P. Salmi and M. Hindmarsh, *Radiation and Relaxation of Oscillons*, *Phys. Rev. D* **85** (2012) 085033 [arXiv:1201.1934] [INSPIRE].

[43] A. Kusenko and M.E. Shaposhnikov, *Supersymmetric Q balls as dark matter*, *Phys. Lett. B* **418** (1998) 46 [hep-ph/9709492] [INSPIRE].

[44] K. Enqvist and J. McDonald, *The dynamics of Affleck-Dine condensate collapse*, *Nucl. Phys. B* **570** (2000) 407 [hep-ph/9908316] [INSPIRE].

[45] S. Kasuya and M. Kawasaki, *Q ball formation through Affleck-Dine mechanism*, *Phys. Rev. D* **61** (2000) 041301 [hep-ph/9909509] [INSPIRE].

[46] Y. Almumin, J. Heeck, A. Rajaraman and C.B. Verhaaren, *Slowly rotating Q-balls*, *Eur. Phys. J. C* **84** (2024) 364 [arXiv:2302.11589] [INSPIRE].

[47] H.-Y. Gao et al., *Boson star superradiance*, *Sci. China Phys. Mech. Astron.* **67** (2024) 260413 [arXiv:2306.01868] [INSPIRE].

[48] E. Clément, L. Vanel, J. Rajchenbach and J. Duran, *Pattern formation in a vibrated two-dimensional granular layer*, *Phys. Rev. E* **53** (1996) 2972.

[49] P.B. Umbanhowar, F. Melo and H.L. Swinney, *Localized excitations in a vertically vibrated granular layer*, *Nature* **382** (1996) 793.

[50] E.J. Copeland, M. Gleiser and H.-R. Muller, *Oscillons: Resonant configurations during bubble collapse*, *Phys. Rev. D* **52** (1995) 1920 [hep-ph/9503217] [INSPIRE].

[51] I. Dymnikova, L. Koziel, M. Khlopov and S. Rubin, *Quasilumps from first order phase transitions*, *Grav. Cosmol.* **6** (2000) 311 [hep-th/0010120] [INSPIRE].

[52] A.B. Adib, M. Gleiser and C.A.S. Almeida, *Long lived oscillons from asymmetric bubbles: Existence and stability*, *Phys. Rev. D* **66** (2002) 085011 [hep-th/0203072] [INSPIRE].

[53] E. Farhi et al., *An oscillon in the SU(2) gauged Higgs model*, *Phys. Rev. D* **72** (2005) 101701 [hep-th/0505273] [INSPIRE].

[54] E. Cotner, A. Kusenko and V. Takhistov, *Primordial Black Holes from Inflaton Fragmentation into Oscillons*, *Phys. Rev. D* **98** (2018) 083513 [arXiv:1801.03321] [INSPIRE].

[55] E. Cotner, A. Kusenko, M. Sasaki and V. Takhistov, *Analytic Description of Primordial Black Hole Formation from Scalar Field Fragmentation*, *JCAP* **10** (2019) 077 [arXiv:1907.10613] [INSPIRE].

[56] J.Y. Widdicombe, T. Helfer and E.A. Lim, *Black hole formation in relativistic Oscillaton collisions*, *JCAP* **01** (2020) 027 [arXiv:1910.01950] [INSPIRE].

[57] Z. Nazari, M. Cicoli, K. Clough and F. Muia, *Oscillon collapse to black holes*, *JCAP* **05** (2021) 027 [arXiv:2010.05933] [INSPIRE].

[58] R. Easther and E.A. Lim, *Stochastic gravitational wave production after inflation*, *JCAP* **04** (2006) 010 [astro-ph/0601617] [INSPIRE].

[59] J.F. Dufaux et al., *Theory and Numerics of Gravitational Waves from Preheating after Inflation*, *Phys. Rev. D* **76** (2007) 123517 [arXiv:0707.0875] [INSPIRE].

[60] S. Antusch, F. Cefalà and S. Orani, *Gravitational waves from oscillons after inflation*, *Phys. Rev. Lett.* **118** (2017) 011303 [*Erratum ibid.* **120** (2018) 219901] [arXiv:1607.01314] [INSPIRE].

JCAP10(2024)082

[61] J. Liu, Z.-K. Guo, R.-G. Cai and G. Shiu, *Gravitational Waves from Oscillons with Cuspy Potentials*, *Phys. Rev. Lett.* **120** (2018) 031301 [arXiv:1707.09841] [INSPIRE].

[62] T. Helfer, E.A. Lim, M.A.G. Garcia and M.A. Amin, *Gravitational Wave Emission from Collisions of Compact Scalar Solitons*, *Phys. Rev. D* **99** (2019) 044046 [arXiv:1802.06733] [INSPIRE].

[63] T. Hiramatsu, E.I. Sfakianakis and M. Yamaguchi, *Gravitational wave spectra from oscillon formation after inflation*, *JHEP* **03** (2021) 021 [arXiv:2011.12201] [INSPIRE].

[64] W. Hu, R. Barkana and A. Gruzinov, *Cold and fuzzy dark matter*, *Phys. Rev. Lett.* **85** (2000) 1158 [astro-ph/0003365] [INSPIRE].

[65] J. Ollé, O. Pujolàs and F. Rompineve, *Oscillons and Dark Matter*, *JCAP* **02** (2020) 006 [arXiv:1906.06352] [INSPIRE].

[66] M. Kawasaki, W. Nakano and E. Sonomoto, *Oscillon of Ultra-Light Axion-like Particle*, *JCAP* **01** (2020) 047 [arXiv:1909.10805] [INSPIRE].

[67] E.G.M. Ferreira, *Ultra-light dark matter*, *Astron. Astrophys. Rev.* **29** (2021) 7 [arXiv:2005.03254] [INSPIRE].

[68] M.A. Amin, R. Easther and H. Finkel, *Inflaton Fragmentation and Oscillon Formation in Three Dimensions*, *JCAP* **12** (2010) 001 [arXiv:1009.2505] [INSPIRE].

[69] M.A. Amin and D. Shirokoff, *Flat-top oscillons in an expanding universe*, *Phys. Rev. D* **81** (2010) 085045 [arXiv:1002.3380] [INSPIRE].

[70] M.A. Amin, *Inflaton fragmentation: Emergence of pseudo-stable inflaton lumps (oscillons) after inflation*, arXiv:1006.3075 [INSPIRE].

[71] Y. Sang and Q.-G. Huang, *Stochastic Gravitational-Wave Background from Axion-Monodromy Oscillons in String Theory During Preheating*, *Phys. Rev. D* **100** (2019) 063516 [arXiv:1905.00371] [INSPIRE].

[72] S. Antusch and S. Orani, *Impact of other scalar fields on oscillons after hilltop inflation*, *JCAP* **03** (2016) 026 [arXiv:1511.02336] [INSPIRE].

[73] S. Antusch, F. Cefalà and S. Orani, *What can we learn from the stochastic gravitational wave background produced by oscillons?*, *JCAP* **03** (2018) 032 [arXiv:1712.03231] [INSPIRE].

[74] S. Antusch, F. Cefalà and F. Torrentí, *Properties of Oscillons in Hilltop Potentials: energies, shapes, and lifetimes*, *JCAP* **10** (2019) 002 [arXiv:1907.00611] [INSPIRE].

[75] M. Piani and J. Rubio, *Preheating in Einstein-Cartan Higgs Inflation: oscillon formation*, *JCAP* **12** (2023) 002 [arXiv:2304.13056] [INSPIRE].

[76] D. Baumann and L. McAllister, *Inflation and String Theory*, Cambridge University Press (2015) [DOI:10.1017/CBO9781316105733] [INSPIRE].

[77] M. Cicoli et al., *String cosmology: From the early universe to today*, *Phys. Rept.* **1059** (2024) 1 [arXiv:2303.04819] [INSPIRE].

[78] F. Apers et al., *String theory and the first half of the universe*, *JCAP* **08** (2024) 018 [arXiv:2401.04064] [INSPIRE].

[79] S.S. Mishra, E.J. Copeland, R. Mahbub, P.M. Saffin and M. Shafi, *Formation and decay of oscillons after inflation in the presence of an external coupling, Part-II: Analytical Results*, in preparation.

JCAP10(2024)082

[80] R.L. Arnowitt, S. Deser and C.W. Misner, *The dynamics of general relativity*, *Gen. Rel. Grav.* **40** (2008) 1997 [gr-qc/0405109] [INSPIRE].

[81] J.M. Maldacena, *Non-Gaussian features of primordial fluctuations in single field inflationary models*, *JHEP* **05** (2003) 013 [astro-ph/0210603] [INSPIRE].

[82] D. Baumann, *Primordial Cosmology*, *PoS* **TASI2017** (2018) 009 [arXiv:1807.03098] [INSPIRE].

[83] A.R. Liddle and S.M. Leach, *How long before the end of inflation were observable perturbations produced?*, *Phys. Rev. D* **68** (2003) 103503 [astro-ph/0305263] [INSPIRE].

[84] S.S. Mishra, V. Sahni and A.A. Starobinsky, *Curing inflationary degeneracies using reheating predictions and relic gravitational waves*, *JCAP* **05** (2021) 075 [arXiv:2101.00271] [INSPIRE].

[85] A.R. Liddle, P. Parsons and J.D. Barrow, *Formalizing the slow roll approximation in inflation*, *Phys. Rev. D* **50** (1994) 7222 [astro-ph/9408015] [INSPIRE].

[86] R. Brandenberger, *Initial conditions for inflation — A short review*, *Int. J. Mod. Phys. D* **26** (2016) 1740002 [arXiv:1601.01918] [INSPIRE].

[87] S.S. Mishra, V. Sahni and A.V. Toporensky, *Initial conditions for Inflation in an FRW Universe*, *Phys. Rev. D* **98** (2018) 083538 [arXiv:1801.04948] [INSPIRE].

[88] R. Kallosh and A. Linde, *Universality Class in Conformal Inflation*, *JCAP* **07** (2013) 002 [arXiv:1306.5220] [INSPIRE].

[89] R. Kallosh, A. Linde and D. Roest, *Superconformal Inflationary α-Attractors*, *JHEP* **11** (2013) 198 [arXiv:1311.0472] [INSPIRE].

[90] S. Antusch, D.G. Figueroa, K. Marschall and F. Torrentí, *Characterizing the postinflationary reheating history: Single daughter field with quadratic-quadratic interaction*, *Phys. Rev. D* **105** (2022) 043532 [arXiv:2112.11280] [INSPIRE].

[91] F. Finelli and R.H. Brandenberger, *Parametric amplification of gravitational fluctuations during reheating*, *Phys. Rev. Lett.* **82** (1999) 1362 [hep-ph/9809490] [INSPIRE].

[92] D.G. Figueroa and F. Torrentí, *Parametric resonance in the early Universe — a fitting analysis*, *JCAP* **02** (2017) 001 [arXiv:1609.05197] [INSPIRE].

[93] D.G. Figueroa, A. Florio, F. Torrentíand W. Valkenburg, *The art of simulating the early Universe — Part I*, *JCAP* **04** (2021) 035 [arXiv:2006.15122] [INSPIRE].

[94] D.G. Figueroa, A. Florio, F. Torrentíand W. Valkenburg, *CosmoLattice: A modern code for lattice simulations of scalar and gauge field dynamics in an expanding universe*, *Comput. Phys. Commun.* **283** (2023) 108586 [arXiv:2102.01031] [INSPIRE].

[95] G. Floquet, *Sur les équations différentielles linéaires à coefficients périodiques*, *Annales Sci. École Norm. Sup.* **12** (1883) 47.

[96] N.W. McLachlan, *Theory and Application of Mathieu Functions*, Clarendon Press (1947).

[97] M. Abramowitz and I.A. Stegun, *Handbook of Mathematical Functions with Formulas, Graphs, and Mathematical Tables*, Dover (1964).

[98] *NIST Digital Library of Mathematical Functions*. https://dlmf.nist.gov/, release 1.1.12 of 2023-12-15.

[99] S.S. Mishra, *Cosmic Inflation: Background dynamics, Quantum fluctuations and Reheating*, arXiv:2403.10606 [INSPIRE].

JCAP10(2024)082

[100] G.N. Felder et al., *Dynamics of symmetry breaking and tachyonic preheating*, *Phys. Rev. Lett.* **87** (2001) 011601 [hep-ph/0012142] [INSPIRE].

[101] G.N. Felder, L. Kofman and A.D. Linde, *Tachyonic instability and dynamics of spontaneous symmetry breaking*, *Phys. Rev. D* **64** (2001) 123517 [hep-th/0106179] [INSPIRE].

[102] M. Ibe, M. Kawasaki, W. Nakano and E. Sonomoto, *Decay of I-ball/Oscillon in Classical Field Theory*, *JHEP* **04** (2019) 030 [arXiv:1901.06130] [INSPIRE].

[103] H.-Y. Zhang, *Gravitational effects on oscillon lifetimes*, *JCAP* **03** (2021) 102 [arXiv:2011.11720] [INSPIRE].

[104] D. Cyncynates and T. Giurgica-Tiron, *Structure of the oscillon: The dynamics of attractive self-interaction*, *Phys. Rev. D* **103** (2021) 116011 [arXiv:2104.02069] [INSPIRE].

[105] L. Iacconi, M. Fasiello, J. Väliviita and D. Wands, *Novel CMB constraints on the α parameter in alpha-attractor models*, *JCAP* **10** (2023) 015 [arXiv:2306.00918] [INSPIRE].

[106] T. Damour and V.F. Mukhanov, *Inflation without slow roll*, *Phys. Rev. Lett.* **80** (1998) 3440 [gr-qc/9712061] [INSPIRE].

[107] A.R. Liddle and A. Mazumdar, *Inflation during oscillations of the inflaton*, *Phys. Rev. D* **58** (1998) 083508 [astro-ph/9806127] [INSPIRE].

[108] W.T. Emond, P. Millington and P.M. Saffin, *Boltzmann equations for preheating*, *JCAP* **09** (2018) 041 [arXiv:1807.11726] [INSPIRE].

[109] M.A.G. Garcia et al., *Effects of fragmentation on post-inflationary reheating*, *JCAP* **12** (2023) 028 [arXiv:2308.16231] [INSPIRE].

[110] M.A.G. Garcia and M. Pierre, *Reheating after inflaton fragmentation*, *JCAP* **11** (2023) 004 [arXiv:2306.08038] [INSPIRE].

[111] M.A.G. Garcia and M. Pierre, *Gravitational wave signatures of post-fragmentation reheating*, *JCAP* **09** (2024) 054 [arXiv:2404.16932] [INSPIRE].

[112] S. Kanno, J. Soda and A. Taniguchi, *Search for high-frequency gravitational waves with Rydberg atoms*, arXiv:2311.03890 [INSPIRE].

[113] N. Aggarwal et al., *Challenges and opportunities of gravitational-wave searches at MHz to GHz frequencies*, *Living Rev. Rel.* **24** (2021) 4 [arXiv:2011.12414] [INSPIRE].

[114] A. Berlin et al., *Detecting high-frequency gravitational waves with microwave cavities*, *Phys. Rev. D* **105** (2022) 116011 [arXiv:2112.11465] [INSPIRE].

[115] A. Ito and J. Soda, *Exploring high-frequency gravitational waves with magnons*, *Eur. Phys. J. C* **83** (2023) 766 [arXiv:2212.04094] [INSPIRE].

[116] C. Gatti, L. Visinelli and M. Zantedeschi, *Cavity detection of gravitational waves: Where do we stand?*, *Phys. Rev. D* **110** (2024) 023018 [arXiv:2403.18610] [INSPIRE].

[117] N. Herman, L. Lehoucq and A. Fúzfa, *Electromagnetic antennas for the resonant detection of the stochastic gravitational wave background*, *Phys. Rev. D* **108** (2023) 124009 [arXiv:2203.15668] [INSPIRE].

[118] K.D. Lozanov and V. Takhistov, *Enhanced Gravitational Waves from Inflaton Oscillons*, *Phys. Rev. Lett.* **130** (2023) 181002 [arXiv:2204.07152] [INSPIRE].

[119] K. Jedamzik, M. Lemoine and J. Martin, *Collapse of Small-Scale Density Perturbations during Preheating in Single Field Inflation*, *JCAP* **09** (2010) 034 [arXiv:1002.3039] [INSPIRE].

JCAP10(2024)082

[120] R. Easther, R. Flauger and J.B. Gilmore, *Delayed Reheating and the Breakdown of Coherent Oscillations*, *JCAP* **04** (2011) 027 [arXiv:1003.3011] [INSPIRE].

[121] J. Martin, T. Papanikolaou, L. Pinol and V. Vennin, *Metric preheating and radiative decay in single-field inflation*, *JCAP* **05** (2020) 003 [arXiv:2002.01820] [INSPIRE].

[122] T. Andrade et al., *GRChombo: An adaptable numerical relativity code for fundamental physics*, *J. Open Source Softw.* **6** (2021) 3703 [arXiv:2201.03458] [INSPIRE].

[123] X.-X. Kou, C. Tian and S.-Y. Zhou, *Oscillon Preheating in Full General Relativity*, *Class. Quant. Grav.* **38** (2021) 045005 [arXiv:1912.09658] [INSPIRE].

[124] J.C. Aurrekoetxea, K. Clough and F. Muia, *Oscillon formation during inflationary preheating with general relativity*, *Phys. Rev. D* **108** (2023) 023501 [arXiv:2304.01673] [INSPIRE].

[125] D. del-Corral, P. Gondolo, K.S. Kumar and J. Marto, *Revisiting primordial black holes formation from preheating instabilities: the case of Starobinsky inflation*, arXiv:2311.02754 [INSPIRE].

[126] E. Tomberg and H. Veermäe, *Tachyonic preheating in plateau inflation*, *JCAP* **12** (2021) 035 [arXiv:2108.10767] [INSPIRE].

[127] N. Koivunen, E. Tomberg and H. Veermäe, *The linear regime of tachyonic preheating*, *JCAP* **07** (2022) 028 [arXiv:2201.04145] [INSPIRE].

[128] S. Antusch, K. Marschall and F. Torrentí, *Characterizing the post-inflationary reheating history. Part II. Multiple interacting daughter fields*, *JCAP* **02** (2023) 019 [arXiv:2206.06319] [INSPIRE].

JCAP10(2024)082